

**Application of Bayesian-based Uncertainty and
Global Sensitivity Analyses to Spacecraft Thermal
Design**

by

Conor B. McMenamin

B.S., Mechanical Engineering
Northeastern University (2012)

Submitted to the Department of Aeronautics and Astronautics

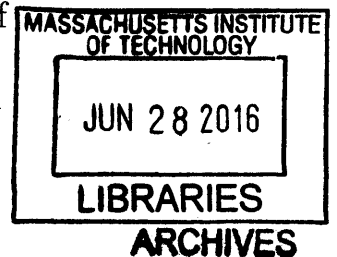
in partial fulfillment of the requirements for the degree of

Master of Science in Aeronautics and Astronautics

at the

MASSACHUSETTS INSTITUTE OF TECHNOLOGY

June 2016



© Massachusetts Institute of Technology 2016. All rights reserved.

Author **Signature redacted** ...
Department of Aeronautics and Astronautics
May 19, 2016

Certified by **Signature redacted**
Rebecca A. Masterson
Research Engineer, Department of Aeronautics and Astronautics
Thesis Supervisor

Certified by **Signature redacted**
Richard P. Binzel
Professor of Planetary Science
Joint Professor of Aeronautics and Astronautics
Thesis Supervisor

Accepted by **Signature redacted**
Paulo C. Lozano
Associate Professor of Aeronautics and Astronautics
Chairman, Graduate Program Committee

Application of Bayesian-based Uncertainty and Global Sensitivity Analyses to Spacecraft Thermal Design

by

Conor B. McMenamin

Submitted to the Department of Aeronautics and Astronautics
on May 19, 2016, in partial fulfillment of the
requirements for the degree of
Master of Science in Aeronautics and Astronautics

Abstract

As satellite design has increased in complexity, the evolution of thermal engineering of spacecraft has plateaued. For years, thermal engineers have used the same principles of designing to stacked worst case scenarios and applying additional margin on top of the already conservative predictions. Recent publications have proposed the use of Bayesian-based probabilistic tools in the design of spacecraft in the effort to avoid overly conservative thermal designs. An issue with utilizing these tools is the typically high computational cost associated with traditional thermal modeling. To help bridge the gap from state-of-the-art to industry standard, this thesis develops a methodology to reduce simulation time and implement these analysis techniques in the industry standard software, Cullimore & Ring Technologies Inc., Thermal Desktop. These design methods are applied to the REgolith X-ray Imaging Spectrometer (REXIS), a student built x-ray spectrometer aboard NASA's OSIRIS-REx mission. Uncertainty analysis shows the area of the main instrument's radiator could have been reduced by 11%, as compared to the design obtained from conventional techniques, and still have a 99% probability of meeting the thermal requirements in all mission phases. Furthermore, global sensitivity analysis results provide insight into the thermal design of the instrument which could have been used to avoid anomalies experienced during integration and testing. Overall, results show that previously established analysis techniques scale to more complex thermal systems and the insights gained from these methodologies can significantly reduce thermal overdesign.

Thesis Supervisor: Rebecca A. Masterson

Title: Research Engineer, Department of Aeronautics and Astronautics

Thesis Supervisor: Richard P. Binzel

Title: Professor of Planetary Science

Joint Professor of Aeronautics and Astronautics

Disclaimer: This material is based upon work supported by the United States Air Force under Air Force Contract No. FA8721-05-C-0002 and/or FA8702-15-D-0001.

Any opinions, findings, and conclusions or recommendations expressed in this material are those of the author and do not necessarily reflect the views of the United States Air Force.

Acknowledgments

First and foremost, I would like to thank the MIT Lincoln Laboratory Lincoln Scholars Program for sponsoring my graduate education. Furthermore, I am thankful to my group leaders at MIT Lincoln Laboratory, Dr. Keith Doyle and Mark Bury, for supporting me through the Lincoln Scholars Program application and while I was away at school.

I thank all my fellow REXIS team members. Thanks to David Carte, Mike Jones, James Chen, Kevin Stout, and Pronoy Biswas. I would like to specially thank Mark Chodas and Laura Bayley. Mark, you are an amazing systems engineer and REXIS is lucky to have you. Laura, thank you for all of the help with class and coding. Without you two, I would not have been able to make it through to the end.

Thank you to my advisors, Professor Richard Binzel and Dr. Becky Masterson, for your guidance on this thesis and my time here at MIT.

Last, but not least, thank you to all of my friends and family who supported me through these tough two years. Thank you Mom and Dad for being there for me and supporting me through all of my endeavors. Thank you to all of my friends who were there to help me de-stress after tough days and celebrate the good days. Thank you Jenn for taking care of me during this last thesis push and keeping me sane throughout the past two years.

Contents

1	Introduction	17
1.1	Background and Motivation	18
1.1.1	Spacecraft Thermal Control System	18
1.1.2	Uncertainty in Thermal Design	22
1.2	Bayesian Approach to Thermal Design	26
1.2.1	Bayesian Uncertainty Background	27
1.2.2	Uncertainty Analysis	28
1.2.3	Global Sensitivity Analysis	30
1.2.4	Review of Recent Research and Research Goals	31
1.3	Thesis Roadmap	32
2	REXIS Background/Overview	35
2.1	REXIS Mission Overview	35
2.2	REXIS Thermal Overview	37
2.2.1	REXIS Instrument Description	38
2.2.2	REXIS Mission Thermal Overview	40
2.2.3	REXIS Thermal Requirements	42
2.3	Spectrometer Thermal Design Overview	44
2.3.1	Thermal Zone 1: Electronics Box	45
2.3.2	Thermal Zone 2: Tower and Titanium Thermal Isolation Layer	46
2.3.3	Thermal Zone 3: CCDs and Radiator	47
2.3.4	Thermal Zone 4: Radiation Cover and Cover Deployment Mech- anism	50

2.4	SXM Thermal Design Overview	52
3	Design Methodology & REXIS Solar X-ray Monitor (SXM) Case Study	55
3.1	Design Methodology	55
3.1.1	Uncertainty Analysis Methodology	56
3.1.2	Global Sensitivity Analysis Methodology	57
3.1.3	Implementation in Thermal Desktop	59
3.2	SXM Design Results	63
3.2.1	Problem Definition	63
3.2.2	Uncertainty Analysis	64
3.2.3	Global Sensitivity Analysis	66
3.3	Lessons Learned	69
3.3.1	Global Sensitivity Analysis Convergence	69
3.3.2	Thermal Desktop Specific Lessons Learned	71
3.4	Bayesian-based Design Implementation	72
4	Spacecraft Battery Case Study	75
4.1	Problem Definition	75
4.2	Uncertainty Analysis	79
4.3	Global Sensitivity Analysis Results	81
5	REXIS Spectrometer Case Study	85
5.1	Problem Definition	85
5.2	Surrogate Model Creation	88
5.3	Uncertainty Analysis	92
5.4	Global Sensitivity Analysis	94
5.5	Frangibolt Thermal Vacuum Testing Anomaly	96
6	Conclusion	103
6.1	Thesis Summary	103
6.2	Applicability of Bayesian-based Design Methodology	105

6.3 Contributions and Future Work 106

List of Figures

1-1	MIL-STD-1540E recommended analysis and test margin	23
1-2	TIRS instrument radiator with MLI covering $\approx 60\%$ of the surface area [1]	25
1-3	Integrated laser transmitter instrument radiator on the CALIPSO satellite [2]	26
1-4	Comparison of analysis predictions to in flight temperatures [3]	27
1-5	Probability density functions representing differing states of knowledge	28
1-6	Thesis roadmap	32
2-1	OSIRIS-REx with Sample Acquisition Arm Extended [4]	36
2-2	Views of REXIS Spectrometer and SXM mounted on OSIRIS-REx [5]	38
2-3	REXIS Spectrometer and SXM shown with major components labeled	39
2-4	OSIRIS-REx Mission Solar Environment [6]	41
2-5	REXIS Spectrometer four thermal zones	44
2-6	Cross sectional view of thermal zone 1: Electronics box	46
2-7	Wedgelock used for conductive thermal path from PCB to electronics box walls	47
2-8	Titanium and Torlon Thermal Isolation Layers (TIL)	48
2-9	Detailed views of thermal zone 3: CCDs and radiator	49
2-10	TiNi FD04 Frangibolt actuator [7] and detailed mid plane view of frangibolt and radiation cover deployment mechanism	50
2-11	Radiation cover heaters and thermostats	51
2-12	Thermal design of SXM	52

3-1	Thermal Desktop Methodology flow chart	60
3-2	Example output code used to write Thermal Desktop QoI output to text file	62
3-3	SXM thermal model created in Thermal Desktop	65
3-4	Probability of meeting SXM thermal requirements versus temperature of T_{OREx} based on 50,000 Monte Carlo samples of the uncertain system	67
3-5	Comparison of global sensitivity analysis results of the main effect Sobol' indices of the SXM for the SDD and SEB QoIs. The parameter variable names are defined in Table 3.1.	68
3-6	Plots of Sobol' indices convergence calculation versus amount of model evaluations for the SXM's SEB and SDD QoIs	70
3-7	Plots of Sobol' indices convergence calculation versus amount of model evaluations for two separate SXM SEB QoI calculations	71
3-8	Comparison of global sensitivity analysis results of the main effect Sobol' indices for different SEB QoIs. The parameter variable names are defined in Table 5.1.	73
3-9	Flow chart of Bayesian-based design methodology, including Thermal Desktop	74
4-1	Thermal model of spacecraft battery with component details	76
4-2	Surrogate thermal model of battery with radiation conductor	81
4-3	Probability of meeting spacecraft battery thermal requirement versus radiator size based on 10,000 Monte Carlo samples of the uncertain system	82
4-4	Global sensitivity analysis results of the main effect Sobol' indices of the spacecraft battery. The parameter variable names are defined in Table 4.2.	83
4-5	Updated global sensitivity analysis results of the main effect Sobol' indices of the spacecraft battery. The parameter variable names are defined in Table 4.2.	84

5-1	REXIS Spectrometer Thermal Desktop model	86
5-2	Full Spectrometer thermal model with surrogate spacecraft thermal model	90
5-3	Radiation conductor to space node, used to represent uncertain emissivity of radiator	91
5-4	Probability of meeting Spectrometer thermal requirements versus radiator size based on 10,000 Monte Carlo samples of the uncertain system	93
5-5	Global sensitivity analysis results of the main effect Sobol' indices of the Spectrometer CCDs and Frangibolt QoIs. The parameter variable names are defined in Table 5.1.	95
5-6	Spectrometer mounted in the thermal vacuum chamber	97
5-7	Temperature of the frangibolt housing, radiation cover, and tower for the duration of the REXIS flight TVAC test	98
5-8	Radiation cover with frangibolt installed prior to TVAC testing . . .	99
5-9	Comparison between model predicted radiation cover heater duty cycle with actual test results	99
5-10	Comparison between updated model predicted radiation cover heater duty cycle with lower G_f and actual test results	100
5-11	Radiation cover post TVAC test after cover actuation has taken place and frangibolt preload no longer present. Cover is closed only by hand	102

List of Tables

1.1	Recommended max and min environmental heat loads for satellites in low Earth orbit	20
2.1	OSIRIS-REx payload instruments and descriptions	36
2.2	REXIS driving thermal mission cases	41
2.3	Spectrometer and SXM temperature requirements/QoIs per component in °C	42
3.1	SXM thermal model uncertain inputs descriptions, density profiles, max, min, and nominal values	65
4.1	Spacecraft battery QoI thermal requirements in °C	76
4.2	Uncertain inputs of spacecraft battery	78
5.1	Uncertain inputs of Spectrometer	89
5.2	Correlation results between surrogate Spectrometer and spacecraft model with full Spectrometer and spacecraft model in °C	91
5.3	Comparison of averaged steady state temperatures between the EM correlated thermal model, updated thermal model, and flight TVAC test results	101

Chapter 1

Introduction

Satellite designs are becoming more complex as advanced technology has made its way to the spacecraft market [8]. As spacecraft design has been evolving to incorporate the state-of-the-art complexities, the design and implementation of thermal solutions to meet these ever changing challenges has plateaued. Spacecraft technologies are becoming smaller and lighter, but dissipate the same, if not more, heat. As the component heat densities have increased, the methods used to design a thermal solution by analyzing to the stacked worst case with additional margin has remained the industry standard. Thermal engineers in industry are understandably risk adverse because of the lack of precise system knowledge during the design phase and the conservative nature of spacecraft design in general [9]. This design approach ensures the thermal requirements of the system are met, but puts undue stress on the other subsystems, schedule, and overall budget [9]. Not all of the thermal overdesign is derived from the thermal engineer's conservatism. Many of the thermal modeling and design decisions originate from a lack of system knowledge. Lack of precise knowledge may manifest itself in the uncertainty of the thermal design parameters or in the uncertainty from the still in-process design of the other subsystems. For example, conservatism can be applied to estimate a thermal control surface's end-of-life (EOL) thermo-optical property. Conversely, a safety factor can/should be applied to the power output from the power system engineer's estimation of heat from a still in design avionics subsystem. This thesis seeks to build upon recent efforts to use each thermal parameter's state

of knowledge in the thermal design, in a probabilistic Bayesian context, as opposed to designing to an unrealistic stacked worst case. Within this proposed design framework, the thermal engineer can gain more insight into the system to appropriately and systematically apply margin and resources. More specifically, this thesis endeavors to bridge the gap between state-of-the-art and industry standard by showing how these tools and design perspective can be implemented on real, computationally intensive, spacecraft applications in the industry standard software.

1.1 Background and Motivation

This section begins with a brief overview of thermal engineering in the aerospace industry. The thermal engineer's role and responsibilities are discussed in order to give context for the case studies presented in later chapters. A major piece of the thermal engineer's role is the design, implementation, and test of the spacecraft's thermal control system (TCS). A description of the TCS is given, along with an overview of the parameters that affect the design of the TCS. Finally, this section presents a discussion on the industry standard practice of applying margin to the TCS and how that margin affects the spacecraft TCS and the satellite as a whole system.

1.1.1 Spacecraft Thermal Control System

Before beginning a discussion on different thermal control systems, it is important to understand why a TCS is needed at all for satellites. Space is a difficult environment to thermally control electronics as the absence of air means the only modes of heat transfer are conduction and radiation. These two modes of heat transfer are represented by Equations 1.1 and 1.2, respectively, where k is conductivity, A is area, $\frac{\Delta T}{\Delta X}$ represents the thermal gradients, ε is emissivity, σ is the Stefan-Boltzmann constant, and T_1 and T_2 are temperatures of radiatively interacting components. All of the thermal energy entering, Q_{in} , and leaving the system, Q_{out} , must be balanced through these two heat transfer modes alone, as shown in Equation 1.3.

$$Q_{conduction} = -kA \frac{\Delta T}{\Delta X} \quad (1.1)$$

$$Q_{radiation} = \varepsilon A_s \sigma (T_1^4 - T_2^4) \quad (1.2)$$

$$Q_{in} = Q_{out} \quad (1.3)$$

Heat entering the system is broken up into 1) environmental heat loads and 2) self generated heat. Environmental heat loads consist of solar flux, planetary reflected solar flux (albedo), or planetary infrared (IR) heat (planetshine). Solar flux and albedo both transfer heat through thermal radiation in the solar wavelengths. Planetshine is the transfer of heat from the planetary body to the orbiting satellite via thermal radiation in the infrared wavelength. For Earth orbiting satellites, all three of these heat loads vary naturally because Earth's slightly elliptical orbit around the sun marginally increases or decreases the solar distance. Solar radiation is proportional to distance from the sun, as shown in Equation 1.4. As the Earth reaches its perihelion, solar flux, and therefore albedo and planetshine increase. The opposite is true for Earth's aphelion. Solar flux, $Q_{SolarFlux}$, can also vary due to increased or decreased solar activity.

$$Q_{SolarFlux} \propto 1/r^2 \quad (1.4)$$

Independent of solar flux variations, albedo naturally varies because various parts of Earth reflect different amounts of solar energy. Deserts naturally have a higher reflectivity than oceans or forests but both of these reflectances can change depending on the presence or absence of higher-reflectance clouds. To encompass all of the bounding minimum and maximum environmental heat load cases, NASA published Table 1.1 which shows the recommended ranges for each heat load for low Earth orbit (LEO) satellites [10].

Self generated heat enters the system from the waste heat produced by the operation of electronics. Electronics are never 100% efficient and these inefficiencies cause

Table 1.1: Recommended max and min environmental heat loads for satellites in low Earth orbit

	Solar Constant (W/m²)	Albedo Factor	Planetshine (W/m²)
Nominal	1368	0.25	256
		0.30	239
		0.35	222
Winter Solstice	1422	0.25	267
		0.30	249
		0.35	231
Summer Solstice	1318	0.25	247
		0.30	231
		0.35	214

heat to be dissipated inside the spacecraft. The self generated heat varies as a function of spacecraft operations. For example, in a typical spacecraft more internal heat generation occurs during a high power communications pass than during a low power charging scenario. All of these heat loads comprise the heat entering the system Q_{in} , as shown in Equation 1.5.

$$Q_{in} = Q_{SolarFlux} + Q_{Albedo} + Q_{Planetshine} + Q_{InternalDissipations} \quad (1.5)$$

All of the heat leaving the system, Q_{out} , leaves through thermal radiation of spacecraft exterior surfaces.

It is the thermal engineer's responsibility to design a TCS that can appropriately reject the environmental and self generated heat while keeping spacecraft components within their operating temperature ranges. The most common tools to control the heat entering and leaving the system are passive thermal control systems (PTCS). Passive thermal control mechanisms are preferred for a TCS due to their simplicity and low size, weight, and power (SWaP). Multi-layer insulation (MLI), radiators, and thermal straps are common examples of passive thermal control devices. Multi-layer insulation is a fundamental PTCS tool used on almost every satellite. MLI consists of many layers of aluminized mylar with outer layers of kapton. The result of stacking these layers provides a set of thermal radiative resistors in series with one another.

These thermal resistors create a very low effective emissivity through the MLI, turning the blanket into a thermal insulator. This effective thermal insulator prevents heat from entering the system from the environment and also prevents heat from leaving the spacecraft. Radiators are typically used to reject heat to the environment in a controlled way. Radiators are usually designed with a surface coating with a low absorptivity α and high emissivity ε . The high ε ensures the radiator can reject heat effectively while the low α reduces the amount of solar environmental flux the radiator absorbs. Sizing the radiator properly is an important task for the thermal engineer. A radiator designed too small will cause the electronics to run hot. Conversely, a radiator that is oversized means the spacecraft will need extra heater power to warm up the electronics, putting an unnecessary strain on the electrical power subsystem. Passive thermal control also includes the intentional conductive coupling or isolating of components. High conductivity thermal straps are used to intentionally conductively couple two components that are far away and need to be structurally decoupled. If isolation is desired, low conductivity materials like titanium or G10 can be used to conductively isolate components [11, 12].

If passive thermal control devices are not adequate to meet the thermal needs of the spacecraft, active thermal control systems (ATCS) can be used. Heaters, thermo-electric coolers (TECs), and fluid loop heat pipes are common examples of active thermal control devices. Heaters convert electrical energy into heat to warm up cold subassemblies in a spacecraft. Conversely, TECs use electricity to create a heat flux between two metals. This heat flux creates a cooling effect which reduces the temperature of one of the metals. TECs are typically used to cool sensitive imagers. Heat pipes use a self contained two phase fluid loop cycle that efficiently transports heat from a hot surface to a cold surface. ATCS gives the thermal engineer more control over spacecraft temperatures but comes at the price of electricity in the case of heaters and TECs and design complexity for the heat pipes [11, 12]. For more information on spacecraft thermal control systems, see Gilmore [11].

1.1.2 Uncertainty in Thermal Design

An important role of the thermal engineer in the design of the TCS is the identification of and designing for uncertainty in the system. The varying levels of environmental heat loads is shown in Table 1.1. PTCS mechanisms in particular have high uncertainties. For example, the effective emissivity of the MLI, commonly referred to as the blanket's ϵ^* (e-star), changes depending on how many layers are in the MLI and on whether the blanket is small or large, flat or uneven, and if it contains dacron meshing or embossed mylar for layer to layer spacing. The higher the ϵ^* , the more heat the MLI allows to flow through it. For radiators or other thermal control surfaces, the thermo-optical properties typically degrade over the mission life. Radiation darkening, outgassing contamination, and atomic oxygen erosion can all cause the surfaces absorptivity to rise, increasing the amount of heat entering the system from the environment. Bolted joint thermal interface resistances have variability based on the size of the bolt used, materials bolted together, and the torque used. All of these uncertainties need to be accounted for in the thermal design to ensure the TCS will keep the spacecraft components within their operational or survival temperature ranges.

To deal with these uncertainties, thermal engineers analyze and design to the stacked worst case hot and cold scenarios. Each uncertain parameter's high or low bound is either associated with a hot or cold case. For example lower, solar flux, minimum spacecraft internal power dissipation, and beginning of life (BOL) thermo-optical properties all drive the spacecraft temperatures lower, creating a cold scenario. A stacked worst case is when all uncertain parameters are chosen with either their associated bounding hot or cold values all at once. If the TCS can meet the thermal requirements under these stacked worst case hot and cold conditions, the design is adequate for all of the more realistic scenarios in between the stacked worst cases.

On top of the stacked worst case results, thermal engineers apply temperature margin. Thermal margin is applied to both the design and testing of components. Figure 1-1 shows the recommended analysis and test margins from military standard

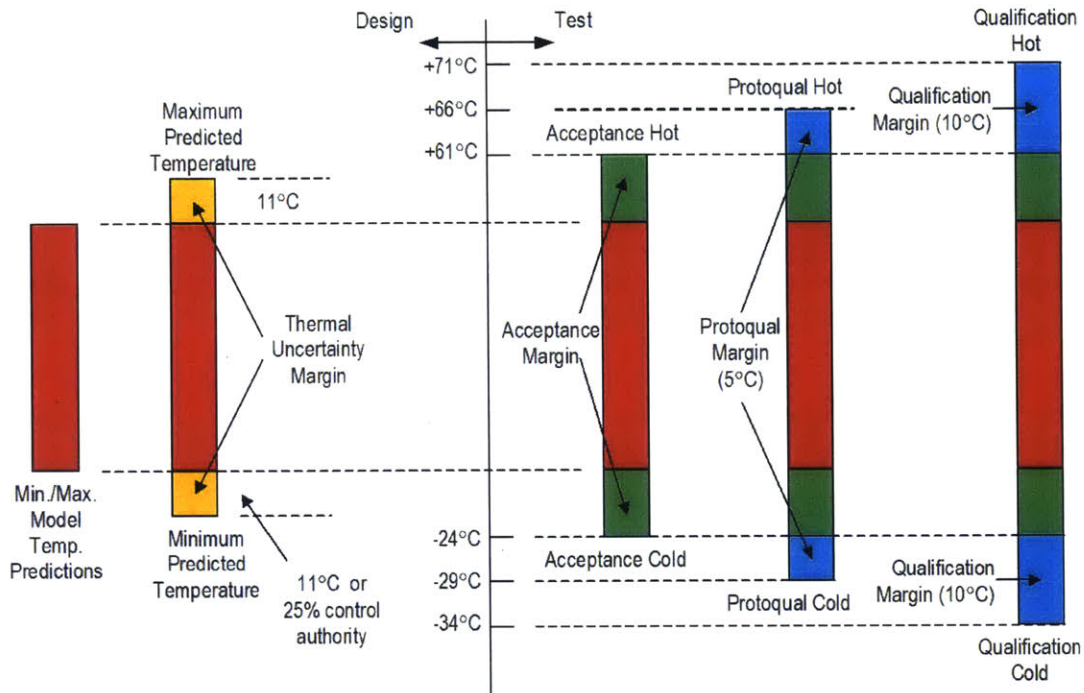


Figure 1-1: MIL-STD-1540E recommended analysis and test margin

MIL-STD-1540 [13]. As shown in Figure 1-1, the standard recommends 11°C of analysis margin on top of the 10°C of Qualification testing margin. Therefore, if the analysis results predict component operational temperatures of -13°C to 50°C in the stacked worst cases, the component would need to be able to operate at -34°C to 71°C. If this wide temperature range is unacceptably high for a component, TCS design changes like increasing radiator size need to be implemented to reduce the maximum temperature predictions. Margin is also applied to ATCS mechanisms by oversizing the heating or cooling capacity of the device. For example, the General Environmental Verification Standard (GEVS) (GSFC-STD-7000) recommends that in the stacked worst case cold scenario, at minimum spacecraft voltage where a heater is producing its minimal amount of heat, the heater shall be oversized such that it operates at less than 70% duty cycle [14]. The 70% heater duty cycle increases the current draw of the circuit by 40% but allows the thermal engineer to only keep 5°C of analysis margin.

Designing the thermal control system to the stacked worst case scenarios and

adding additional analysis and test margin on top of these predicted temperature extremes do ensure the satellite will not violate allowable temperatures limits, but these design and margin allocation practices lead to overdesign. The stacked worst case scenarios produce predicted temperature extremes but no consideration is given to the likelihood or frequency of the conditions aligning in flight as analyzed [15]. These maximum temperature predictions are not normalized by their occurrence duration predicted on orbit. Often, temperature predictions that occur transiently on orbit, even on the order of minutes, are reported as predicted mission worst case temperatures. These components are then tested at elevated temperatures at steady state even though a short transient temperature excursion is more likely to produce graceful degradation rather than catastrophic failure [15].

Overdesigned systems occur in industry because of these conventional practices of designing to a stacked worst case and adding additional margin. Figure 1-2 provides an extreme example of the results from an overdesigned system. The Thermal Infrared Sensor (TIRS) instrument on the Landsat Data Continuity Mission is a cryogenic instrument that was designed on an aggressive schedule [16]. Because of this tight schedule, design decisions were made to accommodate lead time instead of optimization of the system. With this built up conservatism, the thermal vacuum (TVAC) test results concluded that the radiator was oversized. After TVAC testing, 60% of radiator area was covered with MLI to prevent overcooling of the instrument on orbit [16]. Given the unusually aggressive schedule and the 40-50% design margin recommendations for cryogenic systems [17], the overdesigned radiator is not completely unexpected. The schedule and margin notwithstanding, the extra radiator area directly adds mass to the system, but also has the secondary affect of increasing the mass of the structure supporting the radiator.

The TIRS instrument is an extreme example of thermal overdesign but a more typical illustration is given by the Integrated Laser Transmitter (ILT) LIDAR instrument, shown in Figure 1-3, on the CALIPSO satellite. The ILT is designed with an integrated radiator to bias the instrument cold and separate survival and operational heater circuits to warm up the lasers. The radiator size is designed to meet

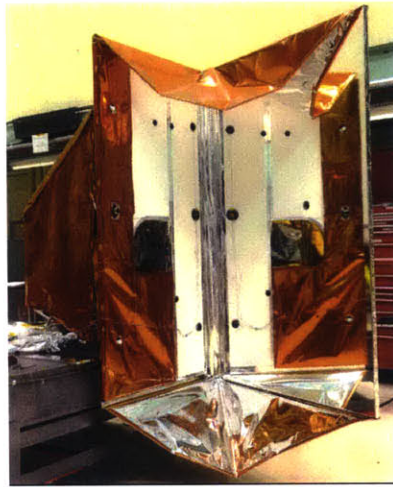


Figure 1-2: TIRS instrument radiator with MLI covering $\approx 60\%$ of the surface area [1]

the thermal requirements for a stacked worst hot case. For the cold cases, the instrument has a 50 W survival heater and a 20 W operational heater to get the laser to operational temperature range before lasing. During satellite-level TVAC testing, it was discovered that power dissipation was lower than expected, and the operational heater was inadequate to overcome the cooling effects of the radiator. Post TVAC it was determined that the radiator area was oversized by 21.5% [18]. To address this overcooling issue, the CALIPSO team decided not to cover part of the radiator area with MLI, and instead use both the operational and survival heaters simultaneously to warm up the lasers enough for operation. With this heater solution, the oversized radiator means not only extra mass, but also extra power draw from the electrical power subsystem.

Although the TIRS and CALIPSO cases show thermal overdesign, it is important to evaluate the effectiveness of thermal control system designs over a broader range of missions. Studying four radiator designs on the LRO, GPM, and ATLAS missions, Garrison concluded that adding 5°C of analysis margin can increase radiator sizing by up to 8% and survival heater power by up to 20% [3]. Since this analysis margin is shown to have such an impact on the overall system, it is important to determine whether this conventional practice of margin allocation is necessary. In

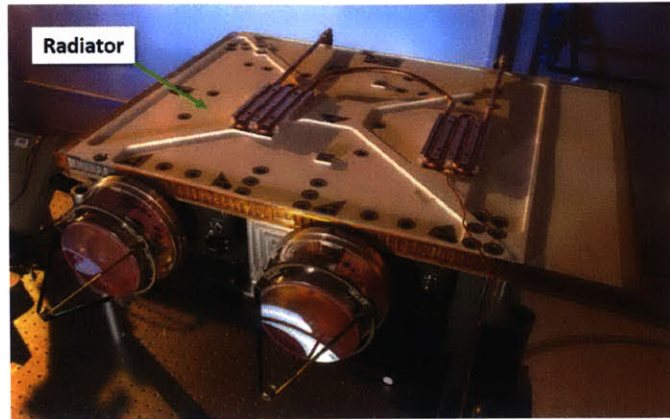


Figure 1-3: Integrated laser transmitter instrument radiator on the CALIPSO satellite [2]

practice, radiators are typically used to control the temperature of spacecraft electronics. Figure 1-4 shows a histogram of the difference between predicted hot stacked worst case temperature extremes and temperatures observed on orbit for the electronics of six NASA missions launched from 2001 to 2010. In the figure, Quadrant I shows the percentage of mission life where the on orbit temperatures are greater than the predicts, and Quadrant II shows when the observed temperatures are less than the predicts. Based on the distribution from the figure, traditional modeling practices produce models that are overly conservative. Most model predicts are over 10°C hotter than the observed on orbit temperatures, meaning the thermal system is designed to an unrealistically conservative case [3]. Therefore, better understanding of model uncertainties can help reduce the overdesign of satellite thermal control systems.

1.2 Bayesian Approach to Thermal Design

An alternative approach to the conservative conventional design methodology incorporates Bayesian-based uncertainty and global sensitivity analyses, examples of which include recent publications by Stout [5] and Thunnissen [19]. Section 1.1 discusses the classic conventional approach to thermal design. Evidence is presented that shows room for improvement over designing to a stacked worst case and adding

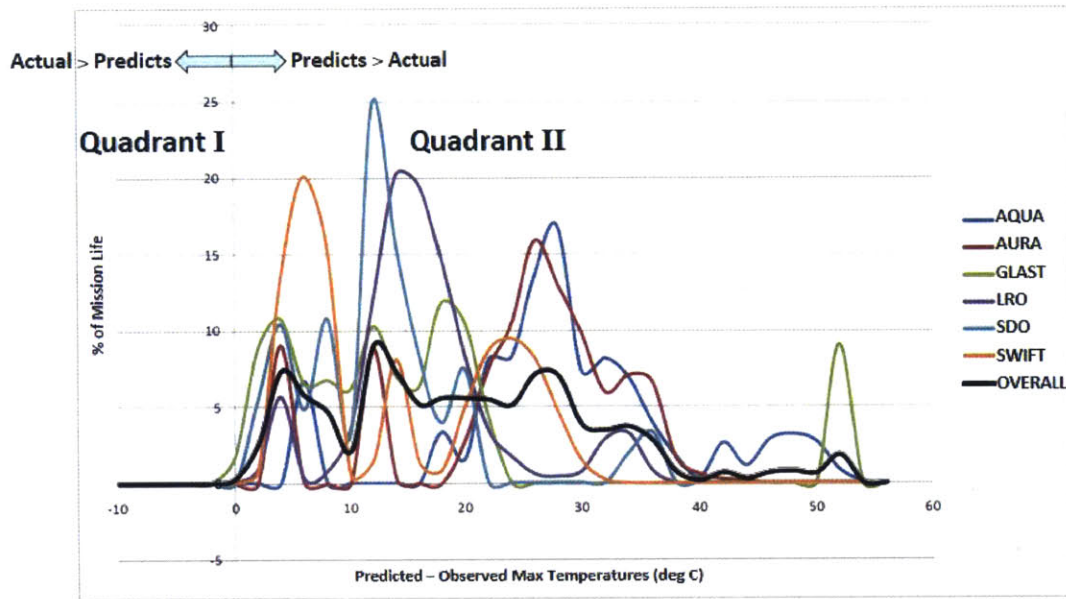


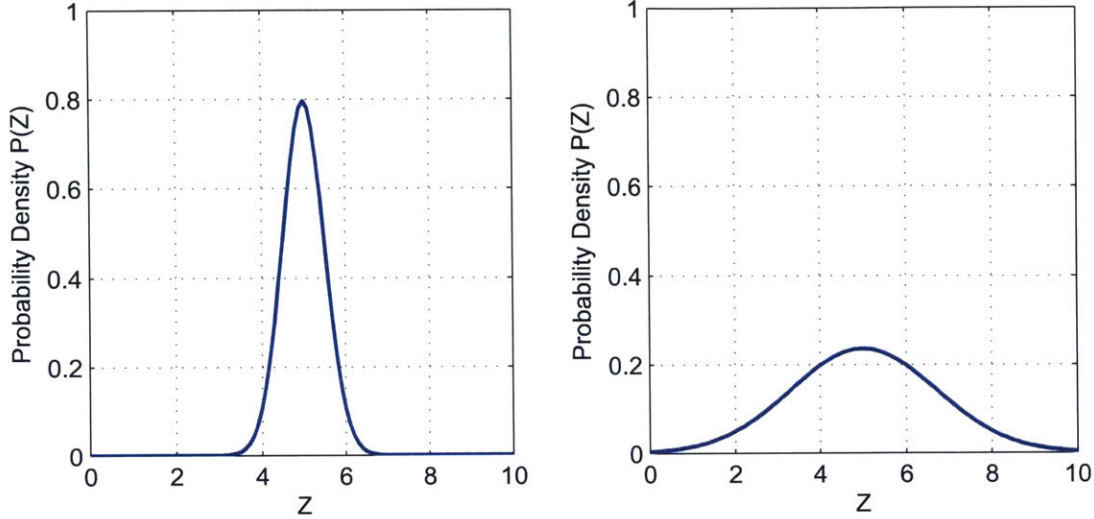
Figure 1-4: Comparison of analysis predictions to in flight temperatures [3]

significant margin on top of the already conservative results. This section presents a Bayesian design approach to help reduce the overdesign caused by conventional techniques. Bayesian concepts are briefly discussed and these concepts are compared to the conventional framework. Bayesian-based uncertainty analysis and global sensitivity analysis are introduced to show how application of these analyses aides spacecraft thermal design. Finally, the section concludes with a review of recent research in this area and an outline of the thesis contributions, including addressing and solving difficulties in implementation.

1.2.1 Bayesian Uncertainty Background

Before discussing the application of a Bayesian framework to the design of a spacecraft TCS, it is important to have some background on Bayesian probability and how this framework differs from the convention. In industry, thermal engineers generally follow a frequentist probability methodology. In frequentist probability, the uncertain parameters are fixed at constant values. The parameter information is obtained by taking the average of repeated tests¹.

In Bayesian probability, the uncertain parameters are unknown and described



(a) Good state of knowledge, low variance (b) Poor state of knowledge, high variance

Figure 1-5: Probability density functions representing differing states of knowledge

probabilistically as continuous probability density functions (PDF). The test results are fixed instead of the parameters. The parameter distributions are updated using the test results¹. These PDFs probabilistically describe the parameter, including a more accurate representation of the mean and variance. The mean and variance of the PDFs represent the possible range of the parameter as well as the state of knowledge of the parameter. A state of knowledge is how well the parameter is known or understood. For example, a very well known parameter would have a PDF similar to Figure 1-5a, while a very uncertain parameter may be better represented by Figure 1-5b.

1.2.2 Uncertainty Analysis

As discussed in Section 1.1.2, many of the important parameters that affect the temperatures in a TCS naturally vary. Uncertainty analysis is a typical technique that is used to calculate the variance in the model output. Model output is any information produced by the results of a simulation. For example, typical model output for

¹Casella, George. "Bayesian and Frequentists." ACCP 37th Annual Meeting, Philadelphia, PA. Department of Statistics, University of Florida.

thermal models consists of temperatures and heat fluxes. Thermal requirements introduced in Section 1.1 are the component temperature criteria that a TCS is designed to satisfy. Model output that maps directly to the requirements of the system are called Quantities of Interests (QoI). Typical QoIs in the thermal design of spacecraft are battery temperatures, temperatures of sensitive imaging devices, and maximum temperatures of electronic boards. Typically, uncertainty analysis is not performed on all of the model output, but just the critical QoIs.

Applying Bayesian-based uncertainty analysis to the spacecraft thermal design gives the thermal engineer more information earlier on in the design process to help reduce thermal overdesign. For most of the uncertain input parameters, the thermal engineer has good knowledge of the typical average and extremes over which these modeling inputs fall. In creation of the hot and cold stacked worst cases, the thermal engineer ignores the most likely value (average), and instead chooses to evaluate the model with one of the values from either extreme. The other extreme for each parameter is then chosen and the model is reevaluated for the other stacked worst case. This conventional mindset produces two discrete outputs for the thermal engineer to evaluate with no information on the likelihood of either case actually happening in flight. In a Bayesian model, each uncertain input parameter has a unique PDF and model evaluations produce a continuous PDF output. Uncertainty analysis is performed on this Bayesian-based thermal model by propagating the uncertainty through the system by monte carlo sampling the uncertain parameters according to their distributions. These model evaluations produce a continuous distribution of model outcome [20]. The continuous model output includes all of the ranges of possible solutions and probabilities associated with each solution. The two stacked worst case scenarios are represented in the continuous PDF output, but probabilities are associated with these scenarios so the thermal engineer can properly weight them in the design process. This continuous distribution of model output provides the thermal engineer with more information about the design, so that they can apply margin in a system specific manner to help reduce overdesign.

1.2.3 Global Sensitivity Analysis

Global sensitivity analysis (GSA) is a quantitative way for the thermal engineer to gain insight into the effects of the uncertain model parameters. Sensitivity analysis has long been a way for system designers to understand the relative importance of parameter inputs in determining the model output [20, 21, 22]. This analysis is useful for determining which parameters significantly affect the solution and which parameters have a small, if any, affect on the model output. Engineers then use these parameter sensitivities to make more informed decisions on the system design. Typically, sensitivity analysis is performed using calculus-based approaches. A calculus-based approach takes the derivative of the model output Y_j versus a parameter input X_i , $\partial Y_j / \partial X_i$. This approach is not optimal because uncertain parameter variances, in a Bayesian context, are not taken into account, and the engineer needs to decide where to take the derivative, which can induce errors or local maximums or minimums. Therefore, derivatives are only informative at the location selected and do not provide information on the rest of the model output space created by the uncertain parameter inputs [20, 22].

Variance-based global sensitivity analysis provides a solution that overcomes the shortfalls of calculus-based methods. Variance-based GSA decomposes the model variance so that portions of the variance are assigned to each uncertain input model parameter. The input model parameters are then investigated to determine how much each parameter contributes to the total variance of the output. The GSA methodology is particularly effective because it captures the effects of the full range of each input parameter, and is able to show the effects of parameter interactions [20]. Variance-based GSA is a natural follow on to uncertainty analysis because uncertainty analysis calculates the variance in the QoI, while GSA provides the answer to which parameters are causing the most amount of variance. Furthermore, the input parameters for GSA are already defined by a continuous PDF, with a mean and finite variance. The conventional thermal engineering approach is not viable for this GSA technique because the discrete inputs of the stacked worst case analyses create discrete outputs

without variance. Since this GSA technique uses the output variance to perform the sensitivity analysis, the technique is not applicable to a model that does not produce an output without a variance.

1.2.4 Review of Recent Research and Research Goals

This thesis seeks to build upon recent work of applying state-of-the-art uncertainty analysis and global sensitivity analysis to spacecraft thermal systems. This thesis does not attempt to create new numerical techniques, but applies these well proven methods to spacecraft thermal design. Moreover, recent research has been published by Stout [5] and Thunnissen [19] that investigates the applicability of Bayesian-based thermal modeling. Stout and Thunnissen have proven the feasibility, but there are research gaps that need to be reconciled before a transition to industry. Stout's Ph.D. works through uncertainty analysis and variance-based global sensitivity analysis on a thermal model, but does so utilizing a thermal model created in Matlab. Matlab is a powerful engineering tool but is not the industry standard that thermal engineers use for their thermal modeling. The aerospace industry standard thermal software is Cullimore & Ring's Thermal Desktop, which provides a graphical environment for thermal engineers to use the SINDA solver. Thunnissen, on the other hand, does use a SINDA based thermal model for his work, but does not perform a variance-based global sensitivity analysis.

It is important to resolve these research gaps before thermal engineers perform uncertainty and global sensitivity analyses in practice because the time involved to learn new software or implement the methodology as is would be prohibitively long. Thermal Desktop has become the industry standard for good reasons. The software neatly wraps together geometry creation, surface ray tracing, and the power of the well-used SINDA solver all together. Creating a large spacecraft thermal model in Matlab is too time consuming and prone to significant errors. The reason variance-based GSA is not the industry standard is not only because of the use of discrete stacked worst cases, but also because of the high computational cost [20]. Using variance-based GSA in practice, 10^4 model evaluations can be required to estimate the

sensitivity of one input with an uncertainty of 10% [23]. When one model evaluation can take upwards of hours, 10^4 model evaluations seems impossible. Because of this high computational cost, it is important to develop techniques to reduce run times before thermal engineers in industry can implement this methodology.

1.3 Thesis Roadmap

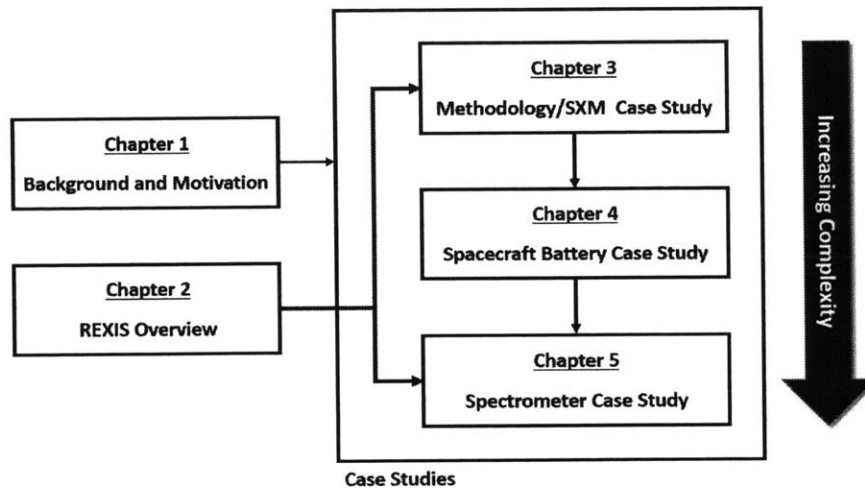


Figure 1-6: Thesis roadmap

This thesis is organized into five chapters. Figure 1-6 shows the thesis roadmap. Chapter 1 is the thesis introduction, including background, motivation, literature review, and thesis goals. Chapter 2 provides an overview of the REgolith X-ray Imaging Spectrometer (REXIS) instrument, a student built x-ray spectrometer aboard NASA’s OSIRIS-REx mission, which is the case study for Chapters 3 and 5. Chapter 3 explains the methodology used to accomplish the thesis goals of bringing the techniques into the industry standard software and reducing model run times. To ensure the methodology is properly implemented, the case study of Chapter 3 is performed on the 65 node REXIS solar X-ray monitor thermal model. The results are compared to the publication of Stout [5], who completed the thermal analysis on a simplified model in Matlab as part of his main Ph.D. case study. Chapter 4 presents a case study on a 650 node spacecraft battery model that is representative of a battery subsystem

on a geosynchronous satellite. Chapter 5 concludes with a complex case study on the 1,500 node REXIS Spectrometer thermal model. The methodology is applied to the Spectrometer and the results are compared with the design obtained from using the industry standard practices. Also, examples are given where this methodology could have benefited the instrument during integration and testing if it had been applied during the design process.

Chapter 2

REXIS Background/Overview

This chapter provides an overview of the OSIRIS-REx mission along with REXIS instrument science products and structural design, including both the REXIS Spectrometer and SXM. Building on the structural design is a discussion of the thermal design, along with thermal requirements for REXIS mission success. A detailed description of the thermal design is critical, as the SXM and Spectrometer are the focus of the case studies in Chapters 3 and 5, respectively. Key instrument design decisions are introduced in this chapter as they affect the Spectrometer global sensitivity analysis results in Chapter 5.

2.1 REXIS Mission Overview

The REXIS instrument is a secondary payload aboard NASA's Origins Spectral Interpretation Resource Identification Security Regolith Explorer (OSIRIS-REx) mission. OSIRIS-REx is the third mission in NASA's New Frontiers program [24]. The mission is led by a principal investigator from the Lunar and Planetary Laboratory at the University of Arizona, and is managed by NASA Goddard Space Flight Center. The bus, shown in Figure 2-1, is built by Lockheed Martin. The primary objective of this mission is to obtain and return a pristine sample of asteroid regolith back to Earth. The asteroid 1999 RQ36, now known as "Bennu" is selected by the OSIRIS-REx science team because of its proximity to Earth, B-type asteroid classification, and

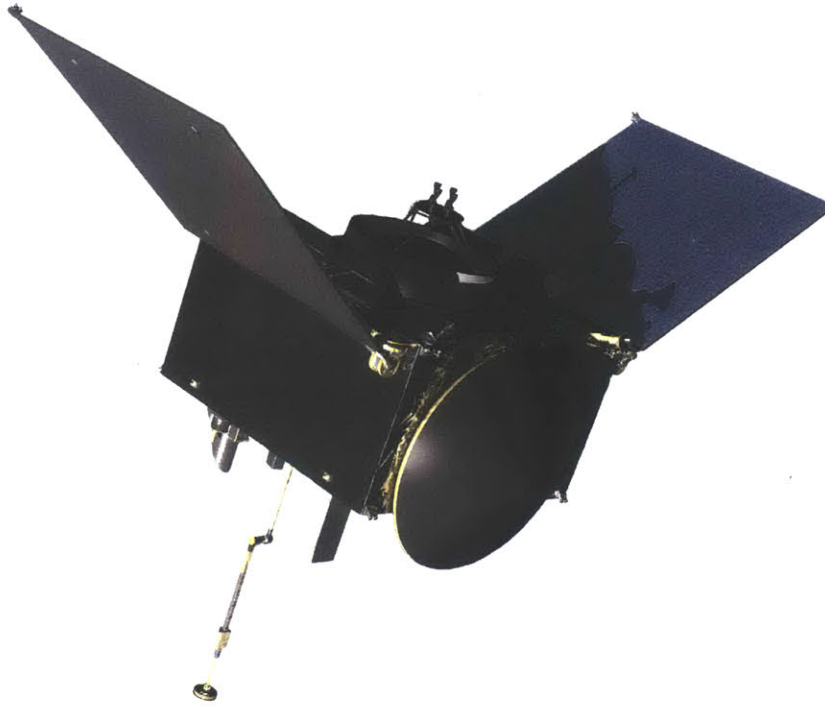


Figure 2-1: OSIRIS-REx with Sample Acquisition Arm Extended [4]

Table 2.1: OSIRIS-REx payload instruments and descriptions

Payload Name		Organization	Mission Function
OCAMS	OSIRIS-REx Camera Suite	Univ. of Arizona	Visible imaging [27]
OLA	OSIRIS-REx Laser Altimeter	Canadian Space Agency	Laser altimetry [28]
OVIRS	OSIRIS-REx Visible and Infrared Spectrometer	NASA Goddard	Near-IR spectroscopy[29]
OTES	OSIRIS-REx Thermal Emission Spectrometer	Arizona State University	Long-IR spectroscopy[30]
REXIS	REgolith X-ray Imaging Spectrometer	MIT & HCO	X-ray spectroscopy [31]

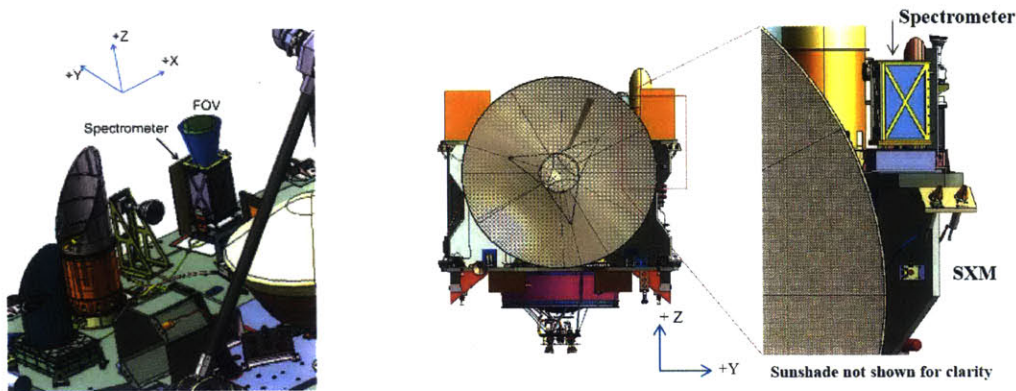
perceived presence of abundant regolith for sampling [25]. B-type asteroids are particularly interesting to the OSIRIS-REx science team because they are believed to be primitive and volatile-rich [26]. There are five secondary payloads on board the bus, built by the University of Arizona, Canadian Space Agency, NASA Goddard Space Flight Center, Arizona State University, and the Massachusetts Institute of Technology. These secondary payloads, a brief description, and their mission functions are listed in Table 2.1.

The Regolith X-ray Imaging Spectrometer (REXIS) is a student collaboration with the Massachusetts Institute of Technology Space Systems Laboratory, MIT Kavli In-

stitute (MKI), Harvard College Observatory (HCO), and MIT Lincoln Laboratory. Almost entirely built by students, REXIS is a risk Class D payload [32] which provides students entering into the aerospace industry a hands on learning experience designing and building flight hardware. The science goals of the REXIS instrument include aiding the OSIRIS-REx mission by using coded aperture imaging x-ray spectroscopy to help determine the elemental abundances of Bennu. Specifically, the REXIS Spectrometer (furthermore referred to as just "Spectrometer" or "the Spectrometer") is designed to observe Bennu in the 0.5-7.5 keV soft X-ray band to measure the elemental ratios of Mg/Si, Fe/Si, and S/Si. These elemental abundance ratios confirm the asteroid classification and may help in sample site selection. In order to perform this X-ray spectroscopy, REXIS takes advantage of the sun's emitted X-rays, which are absorbed and then fluoresced by Bennu. The REXIS Spectrometer collects these fluoresced X-rays using a 2x2 array of charge coupled devices (CCDs). To spatially map the asteroid elemental data, the Spectrometer uses a coded aperture mask with a random hole pattern that casts shadows on the CCD detector array. By deconvolving the shadows on the CCDs created by the hole pattern on the mask, a sky image of the elemental ratios of the asteroid can be reconstructed. To properly calibrate the data observed by the Spectrometer, REXIS includes another smaller instrument named the Solar X-ray Monitor (SXM). The SXM measures the solar X-ray spectra directly via a silicon drift detector (SDD) while asteroid data is collected. With this direct solar data, calibration curves are produced during ground processing to adjust for the transient behavior of the Sun [31].

2.2 REXIS Thermal Overview

This section presents a detailed view and description of the components of the REXIS instrument. This design overview provides a more in depth understanding of the functionality of REXIS and serves to introduce REXIS specific nomenclature. A detailed thermal specific design overview is provided later in Sections 2.3 and 2.4 for the Spectrometer and SXM, respectively. An overview of the mission thermal



(a) Isometric view of Spectrometer (b) View OSIRIS-REx/REXIS from sun (+X)

Figure 2-2: Views of REXIS Spectrometer and SXM mounted on OSIRIS-REx [5]

environment is provided to explain the bounding hot and cold on orbit scenarios. Within these bounding hot and cold scenarios, REXIS specific thermal requirements that are key to mission success are presented.

2.2.1 REXIS Instrument Description

REXIS is comprised of two instruments, the larger Spectrometer and smaller Solar X-ray Monitor. The Spectrometer is mounted on the +Z deck of the spacecraft as shown in Figure 2-2a. The SXM is mounted on the +X spacecraft gusset as shown in Figure 2-2b. During science operations, the +Z deck is asteroid facing and the +X deck is sun facing. The Figure 2-3 shows the Spectrometer and SXM without MLI and with major components labeled. Starting at the bottom and working up the +Z axis, the Spectrometer has an electronics box that houses three electronic boards. The electronic boards communicate with the bus and regulate bus power for the Spectrometer and SXM. The PCBs also electrically interface with the detector assembly mount (DAM), which houses the four MIT Lincoln Laboratory built CCDs. Since the CCDs need to be cold in order to provide sufficient science data, the CCDs are thermally coupled to a cold radiator via a braided copper thermal strap. Two thermal isolation layers (TIL) thermally decouple the CCD assembly from the rest of the structure. The torlon TIL connects the DAM to the bottom panel of the tower

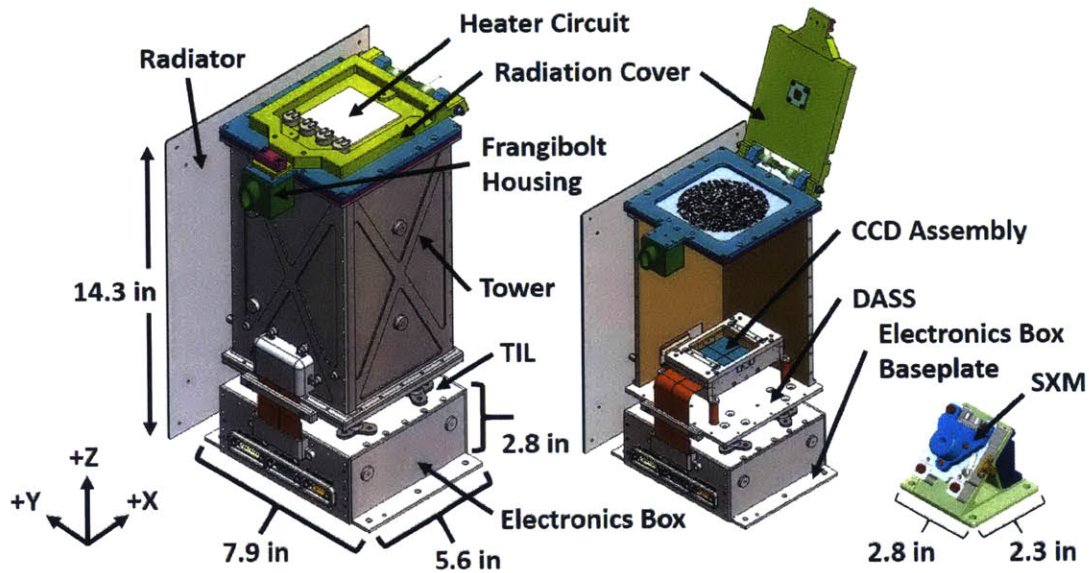


Figure 2-3: REXIS Spectrometer and SXM shown with major components labeled

called the detector assembly support structure (DASS). The titanium TIL is bolted to the top of the electronics box and to the bottom of the DASS and structurally supports the entire tower. The tower houses the CCDs and supports the radiation cover assembly. To prevent radiation damage to the CCDs during the 2 year cruise out to Bennu, the Spectrometer has a radiation cover that closes off the CCDs to the space environment. When the spacecraft reaches Bennu, the cover will open via a one time use actuation mechanism that utilizes a frangibolt and spring hinge system. The frangibolt is mounted inside of the frangibolt housing and is kept warm via a heater circuit on top of the radiation cover. For more information on the design of the Spectrometer, see Carte [33]. For more information on the assembly and integration of the Spectrometer, see Bayley [34].

The SXM is a much smaller and less complex instrument. The SXM has one main bracket that structurally supports the backpack and SXM housing. The backpack and SXM housing both have small electronics boards mounted inside of them. The backpack houses the backpack electronics board (SBB), and the SXM housing provides support for the SXM electronics board (SEB). The backpack electronics board conditions the voltage coming from the Spectrometer for the SEB. The SEB electrically

connects to and controls the SDD, which is cooled using an integrated thermo-electric cooler (TEC) [35].

2.2.2 REXIS Mission Thermal Overview

After the launch of OSIRIS-REx, the satellite takes a two year cruise out to Bennu via an elliptical heliocentric orbit [24]. During this cruise, REXIS is periodically powered on to perform self checkouts and internal calibrations. Since the orbit is eccentric, the thermal environmental loads, i.e. solar flux, seen during the cruise self checkouts and internal calibrations change over the course of the cruise period. The hot case occurs at the orbit's perihelion of 0.773 Astronomical Unit (AU) with a solar loading of ~ 1.3 solar constants, and cold case at the orbit's aphelion of 1.39 AU or ~ 0.72 solar constants, as shown in Figure 2-4. Once OSIRIS-REx arrives at Bennu, the mission enters the Detailed Survey Phase in which the satellite maneuvers itself into a 1 km terminator orbit around Bennu with the +Z deck fixed nadir to the asteroid [36]. The Spectrometer is mounted on this nadir deck such that Bennu is down the boresight of the instrument. By this point, the Spectrometer has actuated the frangibolt and opened its cover to allow the CCDs to begin taking asteroid X-ray data. A mapping of estimated Bennu temperatures and solar reflectance (albedo) is incorporated into the REXIS thermal model. This additional heat load is neglected for the Detailed Survey cold case to be conservative. For the hot case, although the presence of Bennu does provide additional environmental loading to the Spectrometer, once the cover is opened, the heater circuits on the radiation cover and frangibolt housing are powered off, helping to offset this heat load and maintain the CCDs below their science temperature threshold. Table 2.2 summarizes the driving thermal cases for the REXIS instrument per mission phase. For more detailed information about the OSIRIS-REx and REXIS mission thermal scenarios see Stout [5].

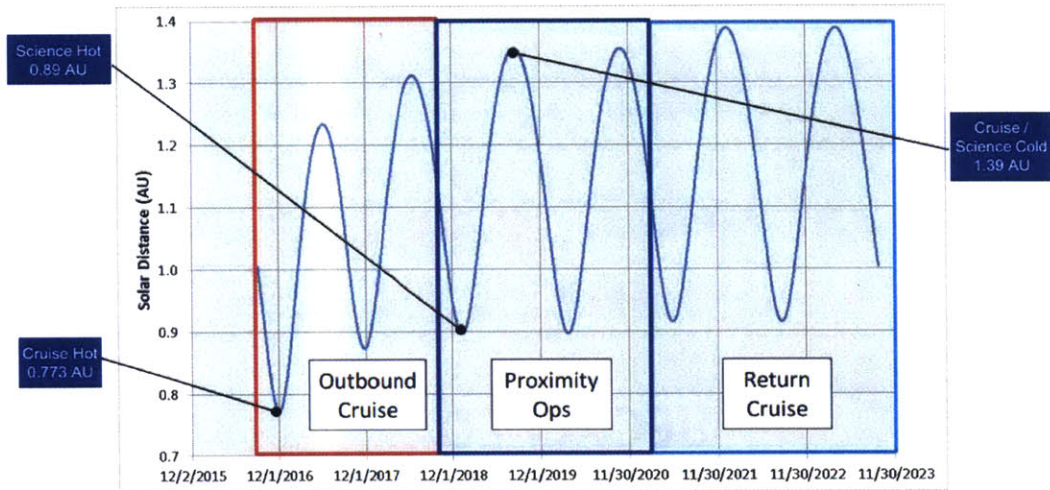


Figure 2-4: OSIRIS-REx Mission Solar Environment [6]

Table 2.2: REXIS driving thermal mission cases

Analysis Case	Case Description	Sun Distance (AU)	Solar Intensity (W/m ²)	Sun Offpoint from +X (deg)	REXIS State	REXIS Cover/Heater
Cruise Phase						
Cruise, Hot	Perihelion	0.773	2322.1	0	On	Closed/On
Cruise, Cold	Aphelion	1.387	700.1	0	Off	Closed/On
Detailed Survey Phase						
DS, Hot 135deg Offpoint	Bennu Perihelion, transient 5 hrs	0.897	1752	45 (+Z)	Off	Closed/On
DS, Hot	Bennu Perihelion	0.897	1752	0	On	Open/Off

Table 2.3: Spectrometer and SXM temperature requirements/QoIs per component in °C

Spectrometer Component Temperature Requirements				
Component	Operational		Non-Operational	
Electronics Boards	-25	85	-35	85
Active PCB Components	-40	110	-40	110
CCDs	-120	-60	-120	60
Frangibolt/Cover Mechanism	-20	80	-20	80
SXM Component Temperature Requirements				
Component	Operational		Non-Operational	
SDD Housing	-40	100	-65	150
SEB	-40	85	-55	85
SDD	-100	-30	-	-

2.2.3 REXIS Thermal Requirements

The Spectrometer thermal design is required to meet the four steady state component temperature criterion listed in Table 2.3. The temperature requirements for the electronics boards and CCDs differ between operational and survival modes of the Spectrometer. During operation, the PCB board temperatures shall not rise above 85°C. This requirement is derived from the temperature limits of the passive board mounted components. For the active board mounted components, each part is thermally analyzed to ensure the derated junction temperature limit is not violated. As per NASA/TP-2003-212242, EEE-INST-002, active board mounted component junction temperatures shall not exceed 110°C or 40°C below manufacturer published maximum junction temperature rating, whichever is lower. This derating ensures the reduction in stress applied to the part during normal operations in order to prolong the expected life [37]. Typically a cold operational analysis is not performed, as the hot operational case is far more stressing, because the component could enter an overheating operational failure mode. Likewise, the failure mechanism for the non-operational cases for the electronics boards becomes a thermostructural issue of potential coefficient of thermal expansion (CTE) mismatch. A thermoelastic analysis

was not completed for the Spectrometer PCBs. Instead, best practice engineering principles were used and testing verified the boards survival from -35°C to 60°C .

The Spectrometer CCDs also have different operational and non-operational thermal requirements. Operationally, the CCDs need to be less than -60°C to collect good science data [31]. At -60°C , there is sufficiently low dark current to meet performance requirements. The low limit on the CCDs for both operational and non-operational modes is set by the thermostructural limit. Engineering model (EM) CCDs were successfully tested down to -120°C and operated again. For the hot non-operational limit, the CCDs shall not exceed the 60°C tested limit. This tested limit is not a driving requirement as the CCDs stay well below this temperature for the duration of the mission.

The temperature requirements of the frangibolt and cover mechanism are critical to ensure high confidence in cover deployment after the two year cold cruise period. The manufacturer published frangibolt temperature ratings are -50°C to $+80^{\circ}\text{C}$ for operation and down to as cold as -80°C for survival. Although frangibolts have flown on and operated in past successful missions [38], this particular miniature model frangibolt has limited flight heritage, having only flown on the DICE cubesat [39] and has not endured a long on orbit storage period before successfully firing. This lack of flight heritage and the temperature dependence actuation time findings in Carte [40] present an increased risk to the contamination effects of the cover deployment due to possible prolonged firing time of the frangibolt. To reduce the uncertainty in frangibolt firing time, and increase the likelihood of the mission critical cover deployment, a requirement of long term frangibolt and cover mechanism temperature to be no colder than -20°C is imposed. The radiation cover heater circuit is designed to satisfy this requirement, but this heater circuit is limited by the bus to 10 W average power usage during cruise.

The SXM thermal design is required to meet the three steady state component temperature criterion listed in Table 2.3. The SDD housing requirements are driven by the manufacturer's allowable temperature limits of the integrated SDD and TEC package. The SDD housing temperature is measured on the hot side of the TEC

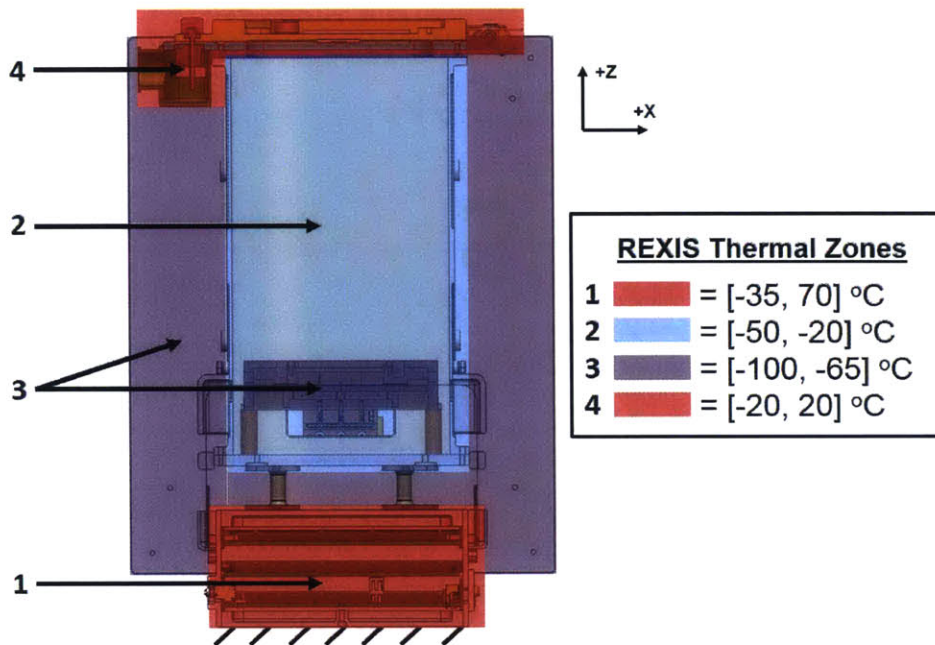


Figure 2-5: REXIS Spectrometer four thermal zones

where it interfaces with the SXM housing. The SEB requirements originate from the maximum and minimum allowable temperature ranges of the board mounted components. The SDD temperature requirements are derived from the limiting detector temperature at which science product degrades. If the SDD temperature requirement is not met, the SXM will not produce usable data, but no component failure will occur. Since the first two SXM thermal requirements are based on component temperature limits, SXM catastrophic failure will occur if the SDD housing or SEB temperature requirements are violated.

2.3 Spectrometer Thermal Design Overview

The thermal design of the Spectrometer breaks up the instrument into four distinct thermal zones. Each zone is designed to operate over different temperature ranges to meet the REXIS thermal requirements/QoIs listed in Table 2.3 and ensure mission success. Figure 2-5 shows the four thermal zones and their on orbit temperature ranges. Thermal zone 1 is a warm zone that is thermally coupled to the spacecraft

interface in order to meet the PCBs thermal requirement. Thermal zone 2 is a colder zone that is thermally isolated from zone 1 in order to reduce the amount of parasitic heat flowing to the CCDs. Thermal zone 3 is the coldest zone that consists of the radiator and CCDs. Thermal zone 3 is further isolated from zones 1 and 2 to meet the CCDs thermal requirement. Lastly, thermal zone 4 is a warm zone on top of zone 2 that uses a heater circuit to keep the frangibolt temperature warm during the Cruise phase. Warming zone 4 without heating up zones 2 and 3 provides for a challenging thermal design and is discussed in this section. This section provides a description of each zone's thermal and mechanical design as these subsystems are closely coupled.

2.3.1 Thermal Zone 1: Electronics Box

The first thermal zone shown in Figure 2-5 is a warm region comprised of the aluminum electronics box and the three Spectrometer electronics boards: the Main Electronics Board (MEB), the Video Board, and the Interface Board. The latter two PCBs are referred to as the Detector Electronics (DE). Figure 2-6a shows a cross section of this first thermal zone. The three boards are mechanically fixed in the electronics box chassis via pairs of Wakefield-Vette wedgelocks, shown in Figure 2-7. The wedgelocks each bolt onto the printed circuit boards (PCBs) via three #2-56 screws. When the boards are properly seated into their corresponding electronics box positions, the drive screw is torqued causing the wedgelock wedges to compress against one another via the inclined planes. This compression provides preload to mechanically fix the PCBs inside the chassis, but also provides a sufficient thermal path for the board generated heat to be conductively dissipated into the electronics box walls, as shown in Figure 2-6b. The electronics box walls bolt together using thirteen #4-40 screws, which are then bolted to the electronics box baseplate using five #4-40 screws. Finally, the electronics box baseplate is then bolted to the spacecraft using six #10-32 bolts. Once the heat has been conducted to the electronics box walls, it conducts down to the electronics box baseplate and then into the spacecraft deck using the thermal path created by the six #10-32 bolts and a wet mount of RTV-566 to the spacecraft. As this first thermal zone relies upon dissipation of the PCB generated

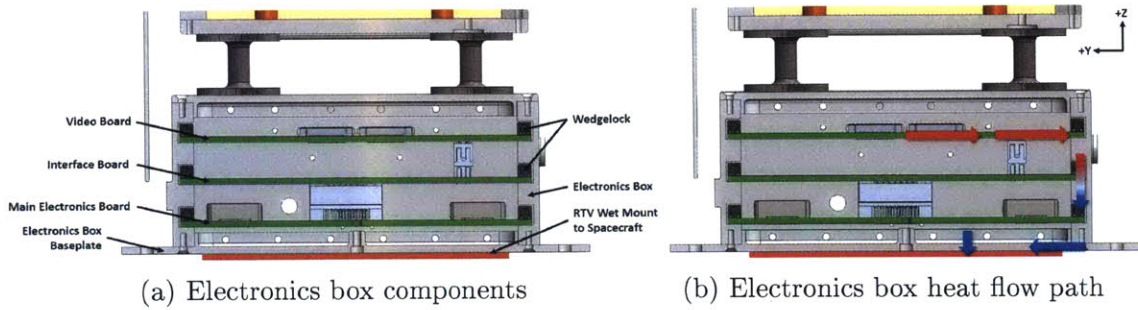


Figure 2-6: Cross sectional view of thermal zone 1: Electronics box

heat into the spacecraft deck, the temperature of this zone is driven by the amount of heat dissipated by the MEB and DE, and the temperature of the spacecraft interface. During instrument level thermal testing, this zone of the Spectrometer is thermal cycled using a temperature controllable plate that simulates the spacecraft interface. The plate is cycled from -25°C to $+50^{\circ}\text{C}$ while the Spectrometer is operating. While the Spectrometer is not operating, the plate is cycled from -35°C to $+60^{\circ}\text{C}$. During TVAC operation, the temperature sensor on the PCBs register near 70°C for the hot case, 15°C below their 85°C limit.

The maximum operational board temperature during testing is near 70°C , but it is still a challenge to keep the active PCB components below their 110°C temperature limit. In the absence of air for convective cooling, for many of the active components, relatively high thermal loads need to be transferred to the PCBs conductively through the small cross sectional chip leads. For these components, the thermal engineer needs to perform an analysis to determine whether an epoxy underfill is necessary. This epoxy underfill bypasses the leads and conductively couples the case of the chip with the PCB.

2.3.2 Thermal Zone 2: Tower and Titanium Thermal Isolation Layer

The second thermal zone shown in Figure 2-5 structurally supports the tower assembly and thermally isolates the tower from the warm electronics box. The thermal zone is comprised of aluminum walls for the tower assembly, and titanium standoffs for

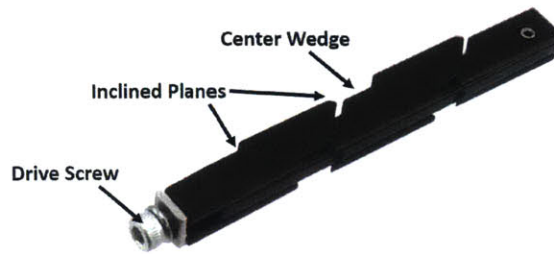


Figure 2-7: Wedgelock used for conductive thermal path from PCB to electronics box walls

the TIL. The main purpose of the tower assembly is to house the CCDs for both mechanical stability and thermal isolation. The tower is structurally supported by four titanium standoffs that are bolted to both the top of the electronics box and the bottom panel of the tower (DASS), with three #8-32 bolts. With the intent of thermally isolating the tower from the electronics box, these titanium standoffs were chosen for their high strength and low thermal conductivity. The titanium standoffs makes up the first TIL shown in Figure 2-8. The tower is approximately 5.5 x 5.3 x 10 inches. The panels are 0.06 inch thick aluminum that bolt to the DASS each with five #4-40 screws and bolt to each other with nine #4-40 screws. As the tower is thermally isolated from the electronics box, the tower temperature is not actively controlled and can not be cycled easily. In instrument level testing the tower temperatures range from -50°C at its coldest to -20°C during the warmest cases.

2.3.3 Thermal Zone 3: CCDs and Radiator

This third zone shown in Figure 2-5, and with more detail in Figure 2-9, includes the DAM, which houses the CCDs, and the radiator assembly. In order to meet the CCD temperature requirements, the third thermal zone isolates the CCDs as much as possible from the rest of the instrument to create the coldest environment attainable. The zone is designed to achieve thermal isolation, but must not compromise structural integrity. The CCDs are mounted to the DASS using four low conductivity torlon standoffs, as shown in Figure 2-8. At the cost of strength, these second layer TIL standoffs have a 95% lower conductivity than the titanium standoffs in the first TIL

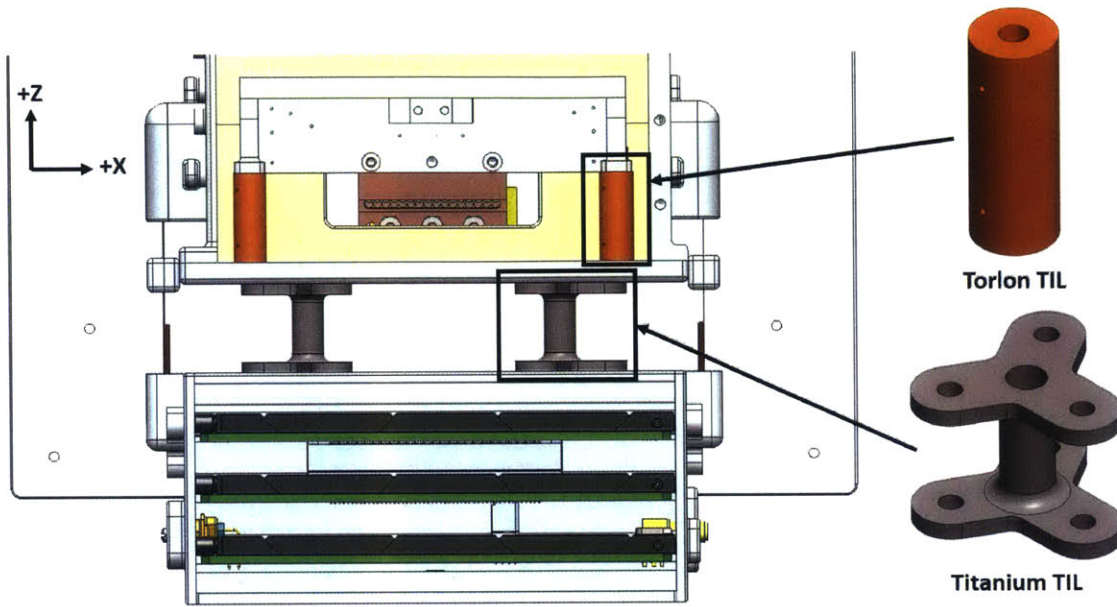


Figure 2-8: Titanium and Torlon Thermal Isolation Layers (TIL)

layer. A lower strength is acceptable here because these torlon standoffs are only supporting the low mass of the DAM. The CCDs are passively cooled by a high conductivity braided copper thermal strap that thermally conducts heat from the CCDs to the radiator. A flexible thermal strap is used to conduct the heat because of the need to structurally decouple the low modes of the radiator from the DAM. To ensure a low thermal resistance, indium foil is used in the bolted joints at the thermal strap to DAM and thermal strap to radiator interfaces. The externally mounted radiator is coated with Z93C55 white paint. This surface coating has a low solar absorptivity α of 0.13 but high emittance ε of 0.92¹. Because of the intentionally high thermal resistance to the rest of the system and the high emissivity of the radiator, this thermal zone operates from -100°C at its coldest to -65°C during the stacked worst hot operational cases.

¹ α and ε values measured by Stinger Ghaffarian Technologies in coordination with NASA GSFC in February, 2015.

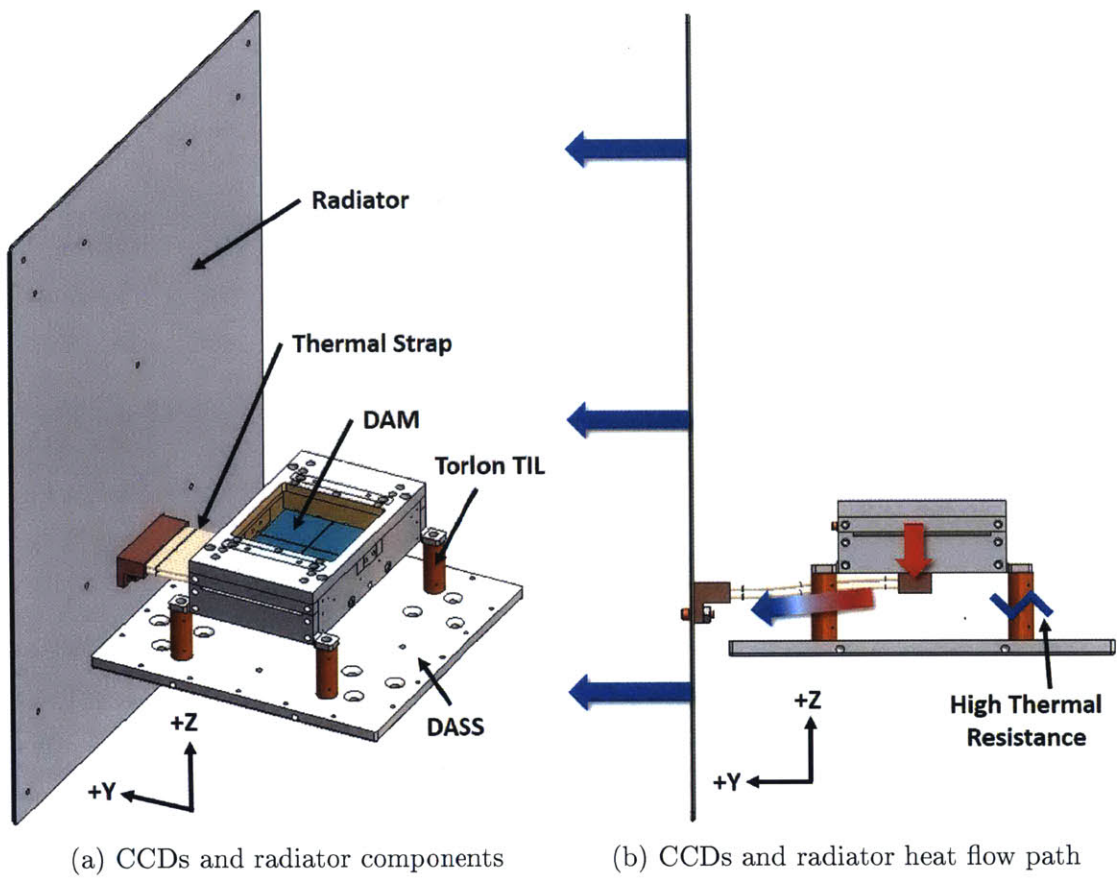


Figure 2-9: Detailed views of thermal zone 3: CCDs and radiator

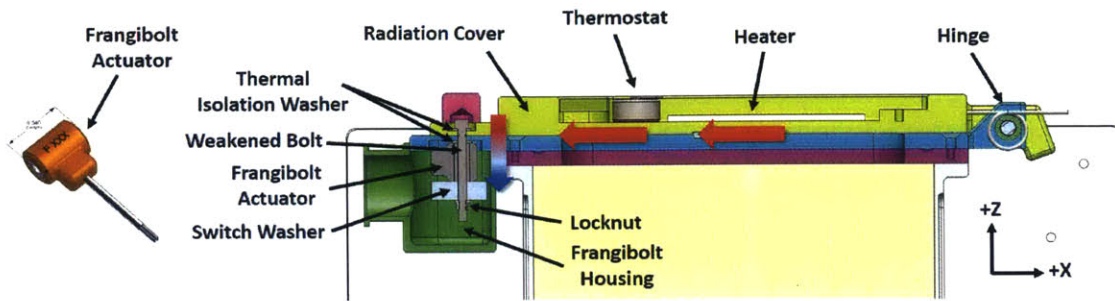


Figure 2-10: TiNi FD04 Frangibolt actuator [7] and detailed mid plane view of frangibolt and radiation cover deployment mechanism

2.3.4 Thermal Zone 4: Radiation Cover and Cover Deployment Mechanism

The fourth zone shown in Figure 2-5 includes the radiation cover, mask frame, frangibolt housing, and frangibolt. This fourth and final thermal zone is a warm temperature region for long term cruise storage of the cover deployment mechanism. The TiNi FD04 frangibolt shown in Figure 2-10 has a temperature dependent shape memory alloy that breaks a weakened bolt when power is applied to the frangibolt's embedded heater. Once the frangibolt breaks, the hinge spring opens the cover to a 110° angle. Although this zone is on top of the cold tower, to reduce the risk of mechanism failure and to increase the confidence in frangibolt actuation time, the deployment system is kept between -20°C to 20°C via the use of a co-located thermostat and heater circuit.

The heater circuit shown in Figure 2-11 is designed to maintain frangibolt temperatures above -20°C for the duration of the cruise phase. During the cruise phase, the REXIS instrument is allocated 10 W average heater power on a separate circuit from main instrument power. This 10 W is used to maintain frangibolt temperatures, but the circuit must be self regulating. To keep the frangibolt at a warm temperature for the cruise duration, the heater circuit's power is dissipated by three 146 ohm kapton heaters wired in parallel. These heaters are bonded down to the aluminum radiation cover using TraBond 2151 epoxy. Epoxy is used to adhere the heaters because the nearly $8\text{ W}/\text{in}^2$ maximum watt density is too high for the 3M 966 pressure sensitive adhesive (PSA) that is typically used to bond kapton heaters. To regulate the heaters,

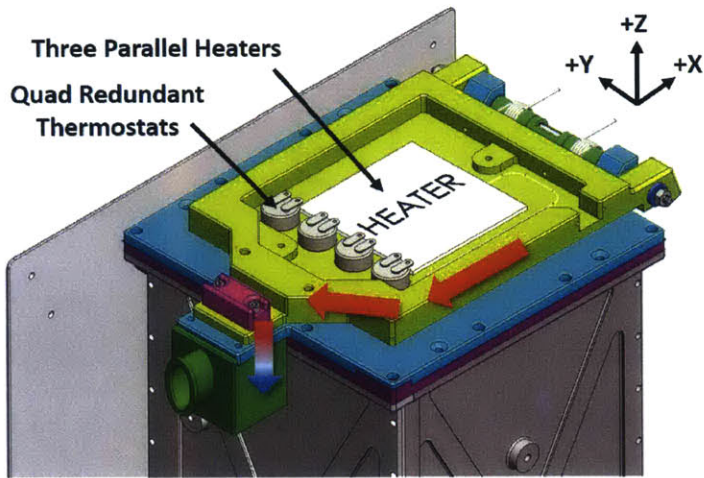


Figure 2-11: Radiation cover heaters and thermostats

four quad redundant Honeywell thermostats, that are wired in paired series-parallel with the heaters, are epoxied nearby. The quad redundancy of the thermostats ensures a two fault tolerant circuit. The setpoints of the thermostats are chosen to ensure the maximum allowable 10 W average heat is generated to keep the actuation mechanism as warm as possible while not exceeding the recommended 70% heater duty cycle.

The conduction path from the heaters to the frangibolt is a key parameter in determining frangibolt temperature. With the thermostats regulating the circuit, the heat is dissipated by the heaters and conducts through the radiation cover and down into the frangibolt, frangibolt housing, and mask frame. Since the heat is being generated on the radiation cover, it needs to conduct through an interface to get to the frangibolt. As shown in Figure 2-10, there are thermal isolation washers guarding the heat from the frangibolt actuation from leaking into the system and slowing actuation time. Unfortunately, these washers also isolate the frangibolt from the radiation cover heaters and make it difficult to accurately predict the temperature of the frangibolt. Therefore, for conservatism, during testing, the frangibolt temperature is inferred by measuring the temperature of the frangibolt housing. For the heater power to conduct down to the frangibolt housing, it needs to conduct through the bolted interface created solely by the preload of the frangibolt bolt. Chapter 5 discusses

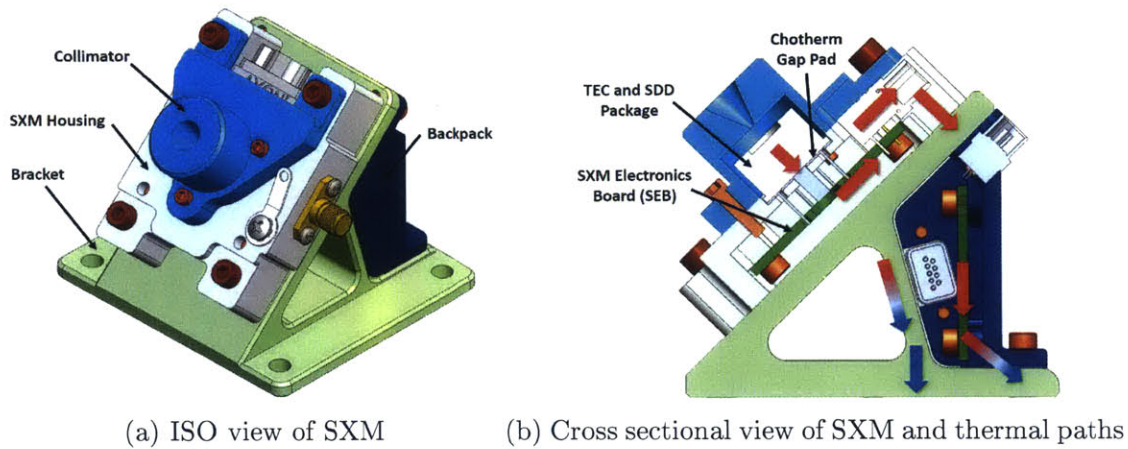


Figure 2-12: Thermal design of SXM

how this design decision to conduct the heat through the frangibolt bolted interface affected the temperature of the actuation mechanism during instrument level thermal testing. For a complete discussion on the details of installing and setting the frangibolt actuator, see Carte [33].

2.4 SXM Thermal Design Overview

This section briefly describes the thermal design of the Solar X-ray Monitor (SXM), shown in detail in Figure 2-12. The SXM is mounted on a sun facing gusset as shown in Figure 2-2b. As mentioned in Section 2.1, the silicon drift detector (SDD) measures the solar spectra directly. The SDD needs to be colder than -30°C in order to have sufficient signal-to-noise ratio. In order to cool the SDD down to this -30°C temperature, a thermoelectric cooler (TEC) is designed into an integrated package with the SDD. The TEC, which is the highest power generating component in the SXM, dissipates its heat into the SXM housing through a thermally conductive CHO-THERM gap pad. Along with the TEC, the other two power dissipating components in the SXM are the SXM electronics board (SEB) and the SXM backpack electronics board (SBB). As shown in Figure 2-12b, all three of these components are conductively coupled to the SXM bracket through the use of bolted joints. The aluminum bracket conductively dissipates the heat from the boards into the spacecraft gusset.

To reduce the environmental heat loading, the SXM is insulated from the solar flux by the spacecraft MLI that covers the gusset. The collimator is exposed to space in order to allow for solar measurements to be taken. For a more detailed description of the SXM thermal design see Stout [5]. For more details on the SXM design and operation see Jones [41].

Chapter 3

Design Methodology & REXIS Solar X-ray Monitor (SXM) Case Study

The goal of this chapter is to provide the methodology for the Bayesian-based thermal design, along with providing a simple case study of the 65 node REXIS Solar X-ray Monitor thermal model to ensure the proper implementation of the methodology. The SXM design study has already been completed by Stout [5] as part of the main case study of his Ph.D. thesis. This chapter presents a recalculation of SXM uncertainty and global sensitivity analysis results utilizing the industry standard software. A comparison between Stout's results and the results presented in this chapter is made to ensure the methodology is properly implemented. Lessons learned from the simple case study are presented and are applied to the more complex case studies in Chapters 4 and 5.

3.1 Design Methodology

Before going through the case study, it is important to understand the methodology behind the uncertainty and global sensitivity analyses. This section details the analyses and the tools used to produce the analysis results. Also, since a major goal of this thesis is to transition these tools to industry, methodology is presented that allows for these analyses to be implemented in Thermal Desktop, the industry standard

software.

3.1.1 Uncertainty Analysis Methodology

The goal of uncertainty analysis is to produce a PDF output distribution that includes all possible model outcomes from any combination of the uncertain input parameters. In the best case scenario, the uncertainty analysis shows the design satisfies the thermal requirements with sufficient confidence. The uncertainty analysis may also show a need for redesign, if thermal requirements are significantly violated, or a need for reduction in uncertainty, if the thermal requirements are satisfied, but not with sufficient confidence.

Before uncertainty analysis is calculated, the simulation model must be created. Equation 3.1 shows the structure of the model:

$$y = \eta(X) = \eta(x_1, x_2, \dots, x_n) \quad (3.1)$$

where y is the model output, X is the set of all uncertain inputs $X = [x_1, x_2, \dots, x_n]^T$, and η is the model. Quantities of Interest (QoI), Q , are a subset of model output y that map to the thermal requirements of the system. In the case for uncertainty analysis, all of the model inputs, $[x_1, x_2, \dots, x_n]$, are described by probability distribution functions, each with a unique mean, variance, and profile. The prior PDFs should be conservatively large to encompass the true value of the parameter, but not too large as to artificially inflate the importance in the uncertainty and global sensitivity analyses. The number of uncertain parameters in the model is referred to as the model's dimensionality. To evaluate the uncertainty analysis, Monte Carlo analysis is a commonly used technique because, as the model's dimensionality increases, the results become more difficult to evaluate by deterministic approaches. A Monte Carlo analysis is performed by repeatedly sampling from each uncertain parameter's distribution. These samples are then used as inputs to the thermal model to produce a model evaluation. A model evaluation is when the model, η , is provided with a set of inputs, X , to calculate model output, y . The expected model output, $E[y]$, given

a set of randomly generated inputs to the model, $\eta(X)$, with probability density of p_X , is then calculated as Equation 3.2:

$$E[y] = E[\eta(X)] = \int \eta(x)p_X(x)dx \quad (3.2)$$

Utilizing the Law of Large Numbers, Equation 3.2 is approximated by Equation 3.3:

$$\bar{\eta}_N = \frac{1}{N} \sum_{i=1}^N \eta(x_i) \quad (3.3)$$

where N is the number of model evaluations, and $\bar{\eta}_N$ is the approximated value of $E[y]$. The model evaluations that are evaluated using the Monte Carlo generated inputs produce a set of model outputs, $Y = [y_1, y_2, \dots, y_N]^T$. Each individual model evaluation produces a discrete model output, y_i . Each subsequent model evaluation produces a different model output, as the inputs to model evaluation i are different than model evaluation $i - 1$. Therefore, the set of model output, Y , creates a probability distribution of all possible outputs and their associated probabilities. This output PDF is used to quantitatively show how well the design satisfies the thermal requirements.

3.1.2 Global Sensitivity Analysis Methodology

The goal of global sensitivity analysis is to quantitatively show which uncertain parameters have the largest affect on the output of the system throughout the entire model space. Chapter 1 discusses the shortcomings of local sensitivity analysis and how GSA overcomes these issues. There are many different types of global sensitivity analysis, but a common GSA technique that is used to guide future research and testing is ANOVA-HDMR. ANOVA-HDMR GSA is used in this thesis because it is a technique that identifies which input parameter's uncertainty is creating the most variance in the output. The thermal engineer can use this information to most efficiently reduce the system's output variance by reducing the uncertainty in the highly sensitive parameters. ANOVA-HDMR stands for analysis of variance - high dimensional model representation. The analysis of variance means the GSA technique

calculates sensitivities by attributing portions of the output variance to each uncertain input. Therefore, the ultimate goal is to calculate how much of the total output variance, V_{total} , can be attributed to each parameter V_i , and the parameters' interactions, V_{ij} . In order to calculate the output variance caused by each parameter, the model must first be decomposed into a high dimensional model representation. A high dimensional model representation is created by breaking up the higher order model, η , into a sum of all of the lower order effects created by each of the model's inputs, η_i , and the input interactions, η_{ij} , η_{ijk} etc, as shown in Equation 3.4 [20, 42, 43]:

$$y = \eta(X) = \eta_0 + \sum_{i=1}^n \eta_i(x_i) + \sum_{i=1}^n \sum_{j>i}^n \eta_{ij}(x_i, x_j) + \dots + \eta_{1,2,\dots,n}(x_1, \dots, x_n) \quad (3.4)$$

This HDMR then leads to variance decomposition shown in Equation 3.5 [20, 42, 43]. Variance decomposition consists of attributing the total variance in the output, V_{total} , to each uncertain input parameter, V_i , and their higher order interactions, V_{ij} .

$$V_{total} = \sum_{i=1}^n V_i + \sum_{i=1}^n \sum_{j>i}^n V_{ij} + \dots + V_{1,2,\dots,n} \quad (3.5)$$

According to Equation 3.5, all of the variance in a model output can be attributed to the variance created by the summation of each uncertain parameter's main effect variance, V_i , along with the higher order variances due to each parameter's interactions with all of the other uncertain inputs, V_{ij} . The main and higher order effects variances are then used to calculate the main effects, Equation 3.6, and total global, Equation 3.7, sensitivities. The main effects and total global effects sensitivities are referred to as the Sobol' indices [20, 42, 43]:

$$S_i = \frac{V_i}{V[Q]} = \frac{V[E[Q|x_i]]}{V[Q]} \quad (3.6)$$

$$S_{Ti} = \frac{E[V[Q|x_{\sim i}]]}{V[Q]} = 1 - \frac{V[E[Q|x_{\sim i}]]}{V[Q]} \quad (3.7)$$

where the sensitivities are calculated for a single scalar QoI, Q . $x_{\sim i}$ represents all of the inputs that are not i . The main effect sensitivity, S_i , is the fraction of variance of Q explained by x_i alone, whereas the total effect sensitivity, S_{Ti} , is everything that is not explained by x_i alone. If no interactions between parameters exist, then $\sum_{i=1}^n V_i = V[Q] = V_{total}$. This equation means that, if there were no higher order interactions between the input parameters, all of the variance in the system is attributed to the summation of the variance caused by each individual input parameter, V_i . If any total effect sensitivity $S_{Ti} = 0$, then that i^{th} parameter is noninfluential and can be fixed anywhere in its distribution without affecting the variance of the output. In general, the sum of the main effects sensitivities are less than or equal to 1, $\sum_{i=1}^n S_i \leq 1$, and the sum of the total effects sensitivities are greater than or equal to 1, $\sum_{i=1}^n S_{Ti} \geq 1$ [20, 42, 43]. For each parameter, a higher Sobol' indice indicates a higher effect on the output for that i^{th} input parameter. The thermal engineer can then rank the input parameters in order of highest sensitivity to lowest sensitivity. Obtaining the main and total effects Sobol' indices quantitatively shows which parameters have the most effect on the variance of the model output, giving the thermal engineer more information about the system to incorporate into the design process.

3.1.3 Implementation in Thermal Desktop

Uncertainty and global sensitivity analyses are very powerful tools to aide in spacecraft thermal design, but the high computational cost of computing the analysis results requires measures to be taken before the methodology can be implemented in Thermal Desktop. The high computational cost is driven from both the large amount of model evaluations required for the analyses, along with the typically long run times of Thermal Desktop model evaluations. Calculating a system's Sobol' indices in practice, 10^4 model evaluations can be required to estimate the sensitivity of one input with an uncertainty of 10% [23]. Furthermore, depending on the size and complexity of the Thermal Desktop model, a single model evaluation may take minutes or hours. To reduce the run times, this section presents a methodology to efficiently perform uncertainty and global sensitivity analyses in Thermal Desktop. This methodology

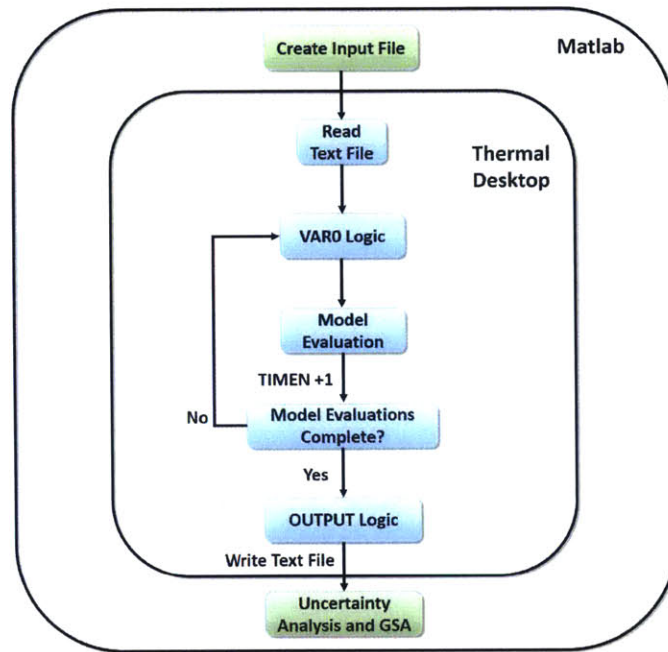


Figure 3-1: Thermal Desktop Methodology flow chart

is called the Thermal Desktop Methodology.

The Thermal Desktop Methodology uses both Matlab and Thermal Desktop, serially. Matlab efficiently samples the uncertain input parameter distributions and creates a text file containing all of the input information for each model evaluation. Thermal Desktop then uses the information in the text file during the repeating model evaluation process. Once all of the model evaluations are complete, Thermal Desktop creates a text file containing just the output QoIs for each model evaluation. This text file is read back into Matlab to perform the uncertainty and global sensitivity analyses as described in Sections 3.1.1 and 3.1.2, respectively.

Figure 3-1 shows a flow chart of the Thermal Desktop Methodology. First, a text file containing all of the sets of uncertain parameters is generated in Matlab using the previously determined parameter bounds and density profiles, with each parameter set to be used for one model evaluation. The OPERATIONS block in Thermal Desktop reads in this text file using the CALL USRFIL command. Care should be taken to insert this code prior to the CALL STEADY command or else the file will not be read during the repeated model evaluations. Next, in the submodel logic, user defined code

written into the VARIABLES 0 logic block commands SINDA to read the first row of the text file, with each column corresponding to predetermined symbols representing each uncertain parameter. The text file read in the VARIABLES 0 logic with the READ command is the text called in the OPERATIONS block. Care should be taken to match the format of the Matlab written text file with the FORMAT call in the VARIABLES 0 logic. SINDA requires a strictly formatted input and will not accept a comma separated value (CSV) file. Furthermore, to allow SINDA to update the parameters for each model evaluation, all of the symbols must be labeled as SINDA registers and output to SINDA. The VARIABLES 0 logic block is used because this code is executed *before* the model is evaluated. The model is then evaluated to generate an output to that specific set of inputs. In a typical Thermal Desktop model evaluation, the run ends here. The model generates output files to capture all of the temperature, heat flux, etc. information and the SINDA session ends. Instead of ending at this step, the methodology utilizes the DTIMES and TIMEND parameters to rapidly increase run times of successive model evaluations. When the DTIMES parameter is set to 1, this integer tells SINDA to run a steady state calculation, but to increment “time” by 1. The TIMEND parameter is then used to set the final “timestep” of the run. Time here is put in quotes because a transient calculation is not performed. This concept of time is used to manipulate SINDA into running many different steady state evaluations sequentially, with each timestep actually being a steady state model evaluation corresponding to a different row in the input file. This SINDA manipulation ensures that all of the model evaluations are calculated in one SINDA session, without the need to communicate back and forth with Thermal Desktop, thereby decreasing the total run time from potentially as high as days to weeks down to minutes, depending on the size of the model and number of model evaluations required. Once the current timestep, TIMEN, has reached TIMEND, the OUTPUT logic block writes user defined temperatures, heat fluxes, heater duty cycles, etc. for each QoI for all of the model evaluations to one text file. Figure 3-2 shows example code used to calculate and store QoI temperatures to be written to the text file. The calculation of the maximum, minimum, and average temperatures

of *Battery*₆ use simple logic and arithmetic, but the NODTRN call is the critical function. This function provides relative location of the temperature information in the SINDA arrays for the Thermal Desktop node numbers. Without this function call, the logic would not work properly. With the temperature information stored in the variables, a WRITE command writes the QoI to the text file. This text file is then read back into Matlab to perform either uncertainty or global sensitivity analysis.

```

C SET NODE NUMBER RANGE:
F DO 15 i=600,674,1
F CALL NODTRN('BATTERY',i,j)
F BATTERY_6_SUM=BATTERY_6_SUM+T(j)
F IF(T(j).GE.BATTERY_6_MAX)BATTERY_6_MAX=T(j)
F IF(T(j).LE.BATTERY_6_MIN)BATTERY_6_MIN=T(j)
F BATTERY_6_NSUM=BATTERY_6_NSUM+1.
F 15 CONTINUE
C CALCULATE AVERAGE TEMPERATURE
BATTERY_6_AVE=BATTERY_6_SUM/BATTERY_6_NSUM

```

Figure 3-2: Example output code used to write Thermal Desktop QoI output to text file

This methodology reduces total run time to allow for the feasibility of uncertainty analysis and GSA to be implemented on models in Thermal Desktop, but the methodology does have limitations. Using the DTIMES parameter only allows for steady state calculations, which limits the application to only scenarios that are in or can be approximated by a steady state solution. Furthermore, the most significant total run time reduction comes from calculating all of the model evaluations in the same SINDA session. Therefore, any change that necessitates dynamic SINDA to be run is not viable. For example, a change in a thermo-optical property requires ray-trace calculations to be rerun, necessitating a need for dynamic SINDA. To avoid these issues, the thermal engineer can approximate the scenario with a slightly modified surrogate model. For instance, although a thermo-optical property cannot be allowed to change, the effect of changing the amount of heat a surface absorbs or emits can be accurately captured using heatloads and radiative resistors, both of which can be allowed to vary within the context of this Thermal Desktop Methodology. Examples of these surrogate modeling techniques are detailed in the case studies of Chapters 4 and 5.

3.2 SXM Design Results

This case study uses a thermal model of the SXM created in Thermal Desktop to design the maximum allowable temperature of the SXM spacecraft interface, T_{OREx} . The Thermal Desktop Methodology presented in 3.1.3 is utilized to reduce run times. To ensure the validity of the results, this case study is chosen because Stout completed the same study as part of his Ph.D. main case study [5]. Stout's results can be considered accurate because the results are compared to and substantiated by test results. Part of the goal of this case study is to determine how well the methodology can be scaled to Thermal Desktop. Therefore, a computationally accurate thermal model of the SXM is created in Thermal Desktop. The SXM thermal model has 65 nodes and allows for thermal gradients. Stout obtained his results using a simplified 5 node thermal model in Matlab that represents each of the 5 major SXM components with a single node. Because each component is only 1 node, this discretization does not allow for thermal gradients within components. With this difference in nodal discretization, minor differences in results are expected. In this section, results from both models are compared, minor differences are explained, and conclusions are drawn.

3.2.1 Problem Definition

Before discussing the Bayesian-based spacecraft interface temperature sizing design results of the SXM, a background on the case study presented in Stout's thesis provides problem definition and context for the reader. As detailed in Chapter 2, the SXM is mounted on the sun facing gusset of the OSIRIS-REx spacecraft. Although this gusset is blanketed with MLI, it receives direct solar flux for most of the mission. Therefore, during the bounding hot mission cases, the gusset can get as warm as 50°C. Since the SXM is a small, very conductively coupled instrument, the temperature of the SXM is driven by the temperature of the gusset/ SXM spacecraft interface, T_{OREx} . During the design phase of the SXM, the maximum temperature of T_{OREx} needed to be negotiated between the REXIS and OSIRIS-REx teams. A lower maximum T_{OREx} is more optimal for the REXIS instrument, but this constraint puts

financial and design constraints on the OSIRIS-REx team. Therefore, a maximum allowable T_{OREx} needs to be designed in which the spacecraft is not significantly burdened, but also such that the SXM still has high confidence of meeting its QoI design requirements listed in Table 2.3. The two driving QoIs for the SXM are the maximum temperatures of the SEB and SDD.

The first step is to identify which parameters are uncertain, and to define density bounds and profiles for each of these uncertain inputs. For this case study, the uncertain parameters and bounds are already chosen and defined by Stout, but the process of picking these parameters is explained to detail the procedure to the reader. The thermal engineer should choose the uncertain parameters by relying on engineering intuition and by evaluating the state of knowledge of each parameter. For example, component mass is not involved in the calculation of a steady state thermal problem. Also, thermo-optical properties of internal surfaces have little change over the course of the mission and are not generally used to transfer significant amounts of heat. Therefore, specific heats and internal thermo-optical properties should remain constant. Conversely, thermal conductors created by bolted joints have known ranges, but do vary from component to component and should be left as an uncertain parameter in the system. The PDF bounds should be chosen conservatively to ensure the actual value is somewhere within the range, but not too large as to artificially increase the importance during GSA. Table 3.1 shows the uncertain parameters identified by Stout for the SXM thermal model and the expected ranges and density profiles for each. All of the major conductive interfaces of the SXM are modeled as uncertain parameters. The power dissipation of the SEB and temperature of the SXM interface are also uncertain parameters. Uniform distributions are selected for all of the parameters because no further information is available in literature for the prior PDFs to allow for profiles with lower variances.

3.2.2 Uncertainty Analysis

With the uncertain parameters selected and prior PDFs created, the PDFs are sampled, in a Monte Carlo analysis, to obtain the sets of inputs for each model evaluation.

Table 3.1: SXM thermal model uncertain inputs descriptions, density profiles, max, min, and nominal values

Parameter #	Description	Variable	Units	Nominal Value	Distribution Type	Minimum	Maximum
1	Conductance between OREx and Bracket	G_b	W/m ² -C	2000	Uniform	100	4000
2	Conductance per screw between bracket and SXM housing	G_{sb}	W/C	0.42	Uniform	0.11	1.32
3	Conductance per screw between pre-amp and SXM housing	G_{sda}	W/C	0.26	Uniform	0.07	0.8
4	Conductance between SDD housing and SXM housing	G_h	W/m ² -C	2000	Uniform	100	4000
5	Conductivity of pins on SDD package	K_p	W/m-C	400	Uniform	350	405
6	Conductance per screw between collimator and SXM housing	G_{sc}	W/C	0.21	Uniform	0.03	0.42
7	SEB SXM Electronics Board power dissipation	Q_{sa}	W	0.20	Uniform	0	0.25
8	Temperature of SXM OREx interface	T_{OREx}	C	40	Uniform	-30	50

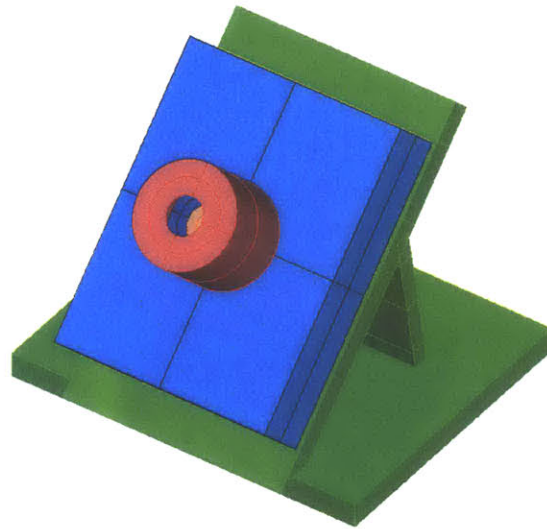


Figure 3-3: SXM thermal model created in Thermal Desktop

The thermal model, shown in Figure 3-3, is used for all of the model evaluations. The model is a relatively simple system with only 65 nodes. Nevertheless, the model does include and allow for thermal gradients within components. Using the Thermal Desktop Methodology explained in Section 3.1.3, 50,000 model evaluations are used to perform the uncertainty analysis, which only takes approximately 1-2 minutes to complete.

The results of the uncertainty analysis are shown in Figure 3-4. Each of the lines represents a cumulative distribution function (CDF) of percent chance of meeting the corresponding thermal requirement conditioned on increasing temperatures of T_{OREx} . The black dashed line representing the confidence threshold is set at 99% for meeting the thermal requirements. The gray line represents the temperature of spacecraft

interface that was set using conventional techniques. The solid lines representing the SDD and SEB QoI are produced using the Thermal Desktop model and methodology. The dashed lines of corresponding color represent the same data published by Stout [5]. For the SDD, the most restrictive QoI, the results correlate well, providing confidence in the Thermal Desktop Methodology. The slight discrepancy between the SEB QoI results is explained by the difference between the two models used. Most importantly, the slope of the two SEB lines, which represents the amount of uncertainty in the system, correlate well to one another. Therefore, the two models are predicting different final temperature values by $\sim 1.5^{\circ}\text{C}$, but the same amount of variance in temperature. The difference in temperature arises from the physics that Stout’s 5 node model is either neglecting or crudely approximating, but is incorporated in the Thermal Desktop model. For example, the main driver between the temperature differences is the thermal gradient within the electronics board. PCBs, being constructed of mostly G10, generally have relatively low conductivities. The Thermal Desktop model represents the SEB with 25 nodes, allowing for a thermal gradient. Conversely, Stout’s model only has 1 node for the SEB, which neglects the effect of in-plane gradients from the center of the board to the edge. This model simplification has the effect of removing resistors from the model, thereby cooling down the model and allowing for higher values of T_{OREx} . The lack of nodal discretization of the SEB does not invalidate Stout’s results, but does provide for minor discrepancies when compared to more a detailed model. This issue is not as prominent in the SDD QoI because the SDD’s small area and high conductivity creates isothermal temperatures for both the Thermal Desktop and Matlab models.

3.2.3 Global Sensitivity Analysis

After the uncertainty analysis is complete, global sensitivity analysis is performed to inform the thermal engineer which parameters are attributing the most amount of variance to the model output. The main and total effects sensitivities are calculated utilizing the numerical techniques described in Saltelli [42]. Again, the GSA results for the Bayesian-based design of the SXM have already been calculated by Stout

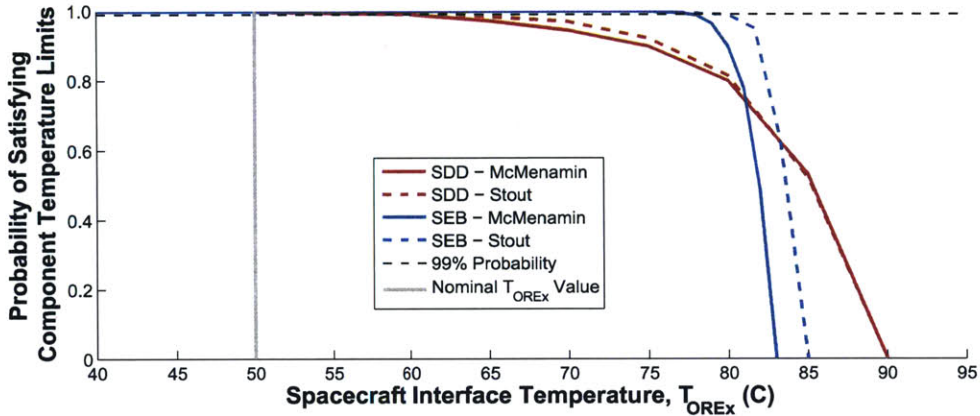
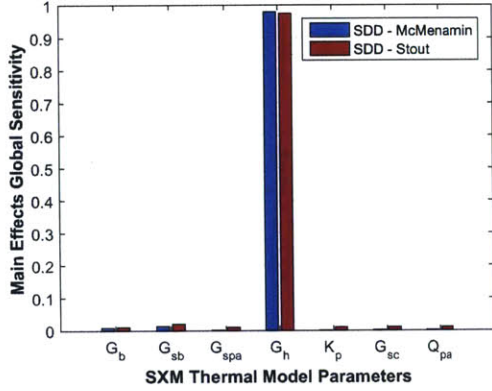


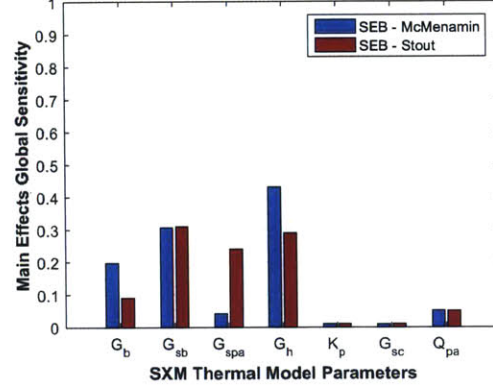
Figure 3-4: Probability of meeting SXM thermal requirements versus temperature of T_{OREx} based on 50,000 Monte Carlo samples of the uncertain system

and recalculated here using the Thermal Desktop model for comparison. The main effects sensitivities for the SDD and SEB SXM thermal requirements are calculated and compared to the results obtained by Stout, shown in Figure 3-5. T_{OREx} is fixed for this sensitivity analysis at 50°C.

Analyzing the global sensitivity analysis of the SDD in Figure 3-5a, the results obtained using the Thermal Desktop Methodology correlate well with the results published by Stout [5]. Figure 3-5a compares the GSA results between the Thermal Desktop and Matlab models for the SDD QoI, and Figure 3-5b compares the results for the SEB QoI. The figures show the main effects global sensitivity, represented by the height of the bars, for each uncertain parameter in the SXM. G_h^{SDD} , the main effect sensitivity of G_h , the conductance between the SDD housing and SXM housing, to the SDD QoI is the dominating parameter, contributing to 97% of the parametric uncertainty. The GSA results of the SEB, shown in Figure 3-5b, correlate well but do have discrepancies that are explained by the difference in models. G_h^{SEB} and G_{spa}^{SEB} , the main effect sensitivity of the conductance of the bolts connecting the SEB to the SXM housing for the SEB QoI, are the two parameters with the highest discrepancies. In the Thermal Desktop model, the power dissipated by the SXM TEC conducts through G_h and K_p , the conductance through the SDD pins, and into the center of the SEB. Because the SEB is discretized in the Thermal Desktop model, instead of a



(a) SDD QoI comparison



(b) SEB QoI comparison

Figure 3-5: Comparison of global sensitivity analysis results of the main effect Sobol' indices of the SXM for the SDD and SEB QoIs. The parameter variable names are defined in Table 3.1.

single node in Stout's model, the thermal gradient in-plane of the PCB is captured. The heat from the TEC dissipated into the center of the PCB creates a relatively large thermal gradient because of the poor thermal conductivity of the PCB. Therefore, it follows such that G_h^{SEB} has a higher sensitivity in the Thermal Desktop model because the uncertainty in this parameter drives the amount of heat entering the PCB, thereby driving the temperature gradient higher or lower. K_p^{SEB} does not have a noticeably higher effect in the Thermal Desktop model because the prior parameter bounds are significantly less uncertain than the bounds of G_h^{SEB} . Furthermore, because the temperature sensitivity of the SEB is being driven, in large part, by the thermal gradient of the Thermal Desktop model, G_{spa}^{SEB} has a relatively lower sensitivity. The sensitivity indices are normalized, meaning the sensitivity results for each parameter are relative to all of the other parameters. Because the thermal gradient is causing G_h^{SEB} to have a higher sensitivity, G_{spa}^{SEB} therefore must have a relatively lower sensitivity when compared to Stout's results. With the discrepancies accounted for, the results of the SXM global sensitivity analysis comparison proves the Thermal Desktop Methodology is properly implemented.

3.3 Lessons Learned

3.3.1 Global Sensitivity Analysis Convergence

Determining the convergence criteria for the global sensitivity analysis is a critical step in the calculation of the Sobol' indices. If the convergence criteria selected is too strict, the analysis will take significantly longer to perform. Conversely, a criteria too loose may result in inaccurate analysis results. For the thermal design of spacecraft, a moderate convergence criteria may be used because the information gained from a sensitivity index is used as a guideline for further research. Whether the sensitivity index is exactly correct or within $\sim 2\%$ of the true answer does not make a difference to the thermal engineer, but may result in thousands or millions of more model evaluations. Therefore, a convergence criteria of a sensitivity index's stability of less than 2.5% is recommended. All GSA results presented in this thesis converge to this criteria.

One of the important lessons learned in performing the SXM case study was the possibly large amount of model evaluations that are required for Sobol' indices convergence. Using variance-based GSA in practice, 10^4 model evaluations can be required to estimate the sensitivity of one input with an uncertainty of 10%, but this amount of model evaluations required is case dependent [23]. The true amount of model evaluations required depends on the amount of variance in the output, the model dimensionality, and, unfortunately, luck. The amount of output variance affects the number of required model evaluations because the variance-based GSA attributes weighted portions of the output variance to each uncertain input. The portions are proportional to the percent of output variance caused by each uncertain input. When the total variance of the output is small, the noise in the Monte Carlo integrator is more significant, causing more model evaluations to be run in order to increase the signal-to-noise ratio in the estimator. When the variance is large, the noise of the Monte Carlo integrator is less significant, and GSA results converge with fewer model evaluations. For example, Figure 3-6 shows a convergence analysis for the SEB and SDD SXM QoIs. Each line in the plots represents a moving stability criteria for

each uncertain parameter. For the calculation to be considered converged, all of the stabilities for each parameter must be under the convergence criteria of 2.5%, as shown by the black dashed line. These Sobol' indices are calculated using the same exact Monte Carlo generated inputs. As shown, the SEB QoI, which has a low variance, does not converge until approximately 1.3 million model evaluations, while the SDD QoI, which has a high variance, converges near 0.4 million model evaluations.

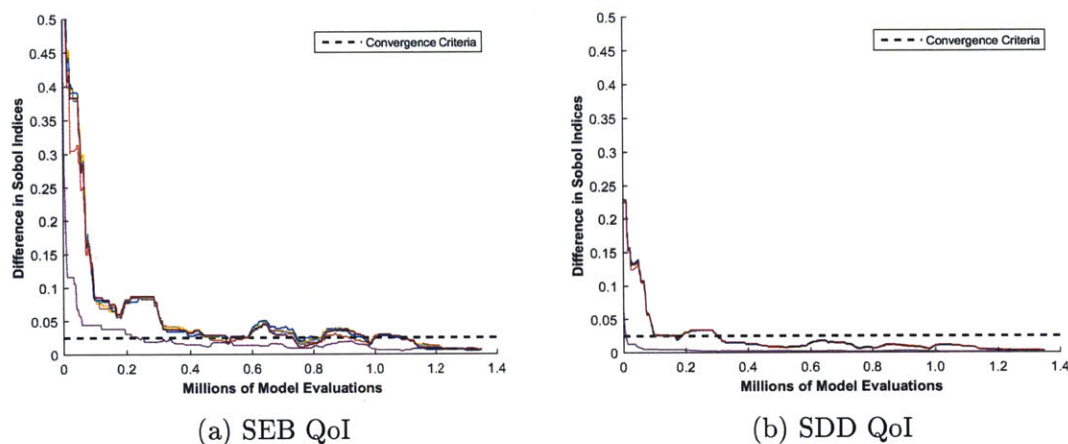


Figure 3-6: Plots of Sobol' indices convergence calculation versus amount of model evaluations for the SXM's SEB and SDD QoIs

The model dimensionality affects the amount of model evaluations required for convergence because each additional input increases the size of the input domain. If the number of samples required to accurately estimate the response over the entire n_i dimensional domain is $n_{s,total}$, then the number of samples required to estimate the main effects sensitivity with model dimensionality, p , is approximately $\frac{p}{n_i} \sqrt{n_{s,total}}$. Therefore, the amount of model evaluations required for convergence increases rapidly with an increasing amount of uncertain parameters [44].

Luck is involved in the amount of model evaluations required for convergence because the Monte Carlo sampling is truly random. From the law of large numbers, it is certain that the correct Sobol' indices are calculated as the amount of model evaluations becomes large, but how many evaluations it takes to get to the convergence criteria is dependent upon the actual numbers generated in the Monte Carlo sampling. If the randomly generated numbers produce indices calculations that are closer to the

actual result, the solution will converge faster. For example, Figure 3-7 shows a convergence analysis for two separate Sobol' indices calculations for the SXM's SEB QoI. Run A and Run B are calculated from completely separately generated 1 million and 5 million model evaluations, respectively. As shown, Run A converges after approximately 0.8 million model evaluations, while Run B does not converge until 2 million model evaluations. The only difference between these two runs that causes the discrepancy in converge is the randomly generated inputs.

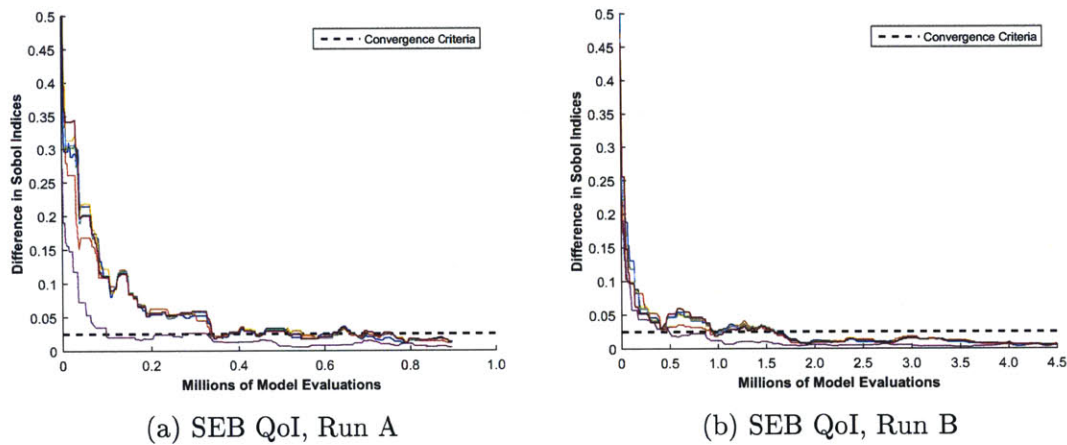


Figure 3-7: Plots of Sobol' indices convergence calculation versus amount of model evaluations for two separate SXM SEB QoI calculations

3.3.2 Thermal Desktop Specific Lessons Learned

The comparison between Stout's and the Thermal Desktop model's uncertainty and global sensitivity analysis results provides useful feedback for future Bayesian-based design studies. Mainly, the thermal engineer needs to take caution in the nodal discretization of the system to accurately capture the details of the model. The results of the SEB QoI clearly show how the lack of nodal discretization can affect the analysis results.

For components that have more than 1 node, the thermal engineer needs to be careful of how the QoI is calculated. For example, Figure 3-8 compares the difference in GSA results of the SEB using QoIs calculated by utilizing the average, minimum,

or maximum temperature of all SEB nodes. Clearly, there is a big discrepancy based on what model output is considered to be the QoI. The minimum temperature node is on the edge of the PCB, where the thermal gradient does not have a large effect. Therefore, if the minimum temperature node is used for the SEB GSA calculations, G_h does not affect that node as much, while G_{spa} is relatively weighted with much higher importance. Conversely, the maximum temperature node is in the middle of the PCB, where the TEC heat is directly conductively coupled. Therefore, the uncertainty in the SEB QoI is dominated by G_h alone because the gradient provides a relatively large temperature variance, compared to the total variance of the SEB. The average temperature of the SEB is used for the comparison in Figure 3-5. Utilizing the average temperature in the GSA calculations averages out the effects of both the minimum and maximum nodal temperature results. Therefore, average temperatures are used in the calculations for the uncertainty and global sensitivity analysis case studies presented in Chapters 4 and 5.

3.4 Bayesian-based Design Implementation

The SXM design case study presented in this chapter is an important validation step to ensure the Thermal Desktop Methodology is properly implemented but, because the modeling is relatively simple and the problem was defined previously, not all of the steps in the full Thermal Desktop included Bayesian-based design methodology could be fully implemented. Figure 3-9 shows a flow chart of the full Bayesian-based design methodology, including Thermal Desktop. First the design problem is defined to scope out the work. For example, this problem definition could be the negotiation over interface temperature, as shown in the SXM case study, or sizing of a radiator, as is demonstrated in Chapters 4 and 5. Next the uncertain parameters of the thermal model are selected and given prior PDF profiles and bounds. The prior PDFs are obtained from published resources, test results, and/or thermal intuition from previous experiences. The priors in Chapter 4 are obtained from published resources while the Chapter 5 priors originate from previous test results. The next

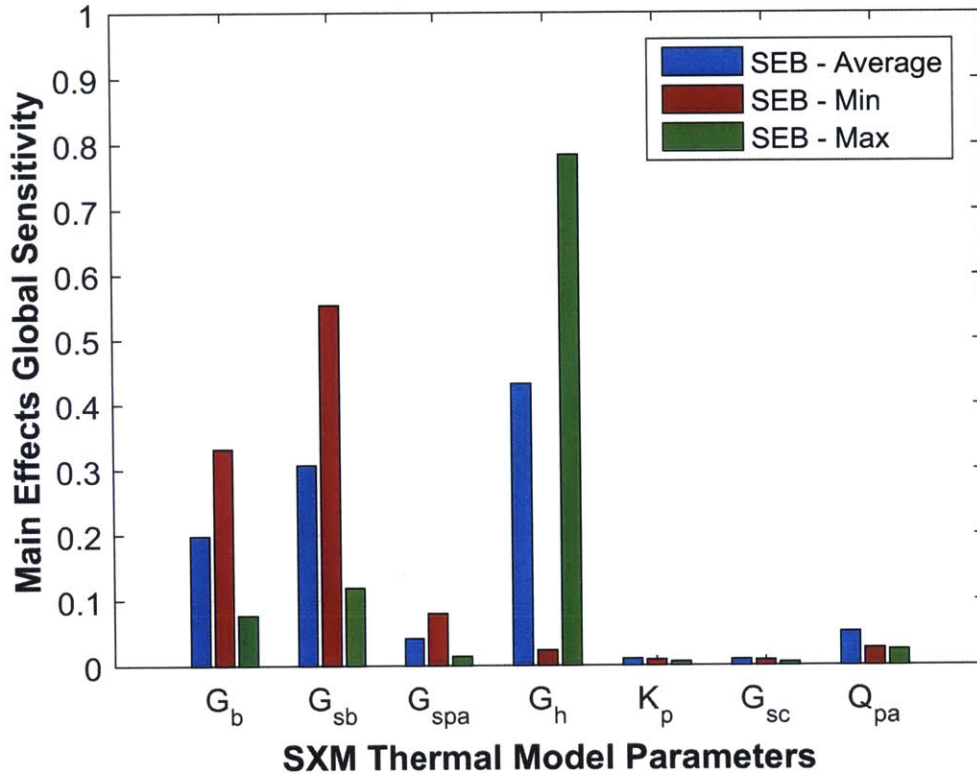


Figure 3-8: Comparison of global sensitivity analysis results of the main effect Sobol' indices for different SEB QoIs. The parameter variable names are defined in Table 5.1.

steps in the methodology are the creation and validation of a surrogate thermal model. As the thermal models become bigger and more complex, so does the need for a surrogate thermal model to reduce the simulation times. Surrogate models are also created in Thermal Desktop, but use different modeling techniques to allow for the Thermal Desktop Methodology presented in Section 3.1.3 to be fully implemented on all of the uncertain parameters. The surrogate model in Chapter 4 only requires slight alterations, while the thermal model in Chapter 5 requires fairly significant modifications. Furthermore, the surrogate models created need to be validated against the full models to ensure accurate results. Once the surrogate models are created, the uncertainty and global sensitivity analyses are performed in Thermal Desktop using the fundamental math and Thermal Desktop Methodology presented in Section 3.1. Finally, the results of the analyses are analyzed to resolve the design problem and

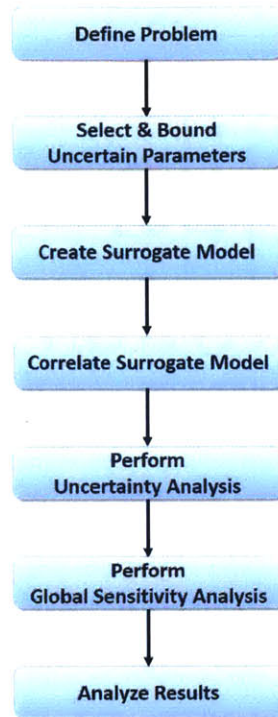


Figure 3-9: Flow chart of Bayesian-based design methodology, including Thermal Desktop

gain more insight into the system. Each step of this full methodology is illustrated, in detail, in the case studies of Chapters 4 and 5.

Chapter 4

Spacecraft Battery Case Study

The goal of this chapter is to demonstrate the Bayesian-based design methodology implemented in Thermal Desktop on a moderately complex 650 node spacecraft battery thermal model as the case study. The spacecraft battery model is a fictional case that is representative of a realistic battery subsystem. The design case study is first defined to provide context for the design problem. Thermal boundary conditions are then given for the uncertainty and global sensitivity analyses. Radiator sizing design results of the uncertainty analysis are compared against the design results obtained using conventional techniques. A global sensitivity analysis using Sobol' indices is performed to gain more insight into the design of the battery subsystem. Finally, the information from the uncertainty and global sensitivity analyses is analyzed to see how this information affects the overall design of the system.

4.1 Problem Definition

This section provides a background on the thermal design of the spacecraft battery subsystem. This case study is chosen because batteries typically have a narrow operational temperature range. This narrow temperature range, along with the criticality of the successful operation of the batteries, leads thermal engineers to be conservative in the thermal design of battery systems. This battery is assumed to be part of the power subsystem for a geosynchronous (GEO) satellite. The GEO satellite orbits at

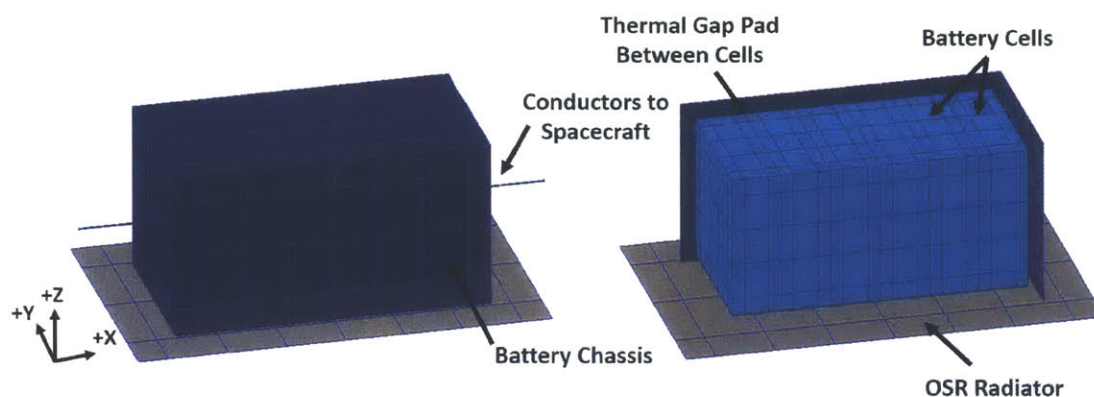


Figure 4-1: Thermal model of spacecraft battery with component details

the equator, i.e. has an inclination of 0 degrees. The battery subsystem is mounted on the south deck of the satellite, with an integrated optical solar reflector (OSR) radiator for cooling and heater circuit for warming. An OSR radiator is chosen because of its high performance and relatively low thermo-optical property degradation rate [11]. The battery subsystem is mounted on the south deck of the GEO spacecraft to reduce the amount of absorbed solar flux throughout the year. The amount of solar flux is, in part, dependent on the current beta angle of the orbit. A beta angle is the angle measurement between the sun vector and orbital plane. The beta angle throughout the year ranges from 23.5° during the winter solstice to -23.5° during the summer solstice, and closer to 0° near the equinoxes. The battery chassis is bolted to the rest of the spacecraft using low conductivity G10 thermal isolation washers to decrease the amount of heat flow to and from the spacecraft. The spacecraft temperature is assumed to vary from -20°C to $+40^\circ\text{C}$. Given these thermal boundary conditions, the thermal engineer needs to design the battery thermal subsystem to ensure the thermal requirements in Table 4.1 are met, with 5°C of margin. For this battery case study, the temperature of the battery cells is the quantity of interest.

Table 4.1: Spacecraft battery QoI thermal requirements in $^\circ\text{C}$

Battery Temperature Requirement		
Component	Operational	
Battery	0	30

With the problem introduced and thermal boundary conditions defined, the thermal model is created to represent the physical system. Figure 4-1 shows the battery thermal model. The system includes six battery cells that are compressed together and thermally connected to one another utilizing thermal gap pads in between the cells. The cells are also connected to the +X, -X, and +Z chassis walls using the thermal gap pads. The aluminum chassis walls are assumed to be bolted together using # 6 bolts. The radiator is bolted to the chassis walls using # 8 bolts. The OSR radiator is represented by the -Z face, which radiates heat to space and absorbs solar flux. The +X and -X walls are conductively coupled to a node representing the temperature of the spacecraft. The chassis is assumed to be covered with MLI, limiting the only thermal interaction between the chassis and spacecraft to the conduction to the spacecraft node.

The two objectives of the thermal design of this battery subsystem are 1) size the radiator of the battery subsystem, and 2) investigate the effects of assumptions made by battery vendor. In this case study, it is assumed that the initial thermal model is created by the battery vendor. The vendor provides the preliminary set of assumptions for the thermal design of the battery subsystem, but since no information is known about the orbital conditions and spacecraft interface, the vendor relies upon their customer's thermal engineer to size the radiator. Therefore, the thermal engineer must take into account all of the uncertainties in the model to conservatively size the radiator to meet the thermal requirements. Furthermore, in sizing the radiator, the thermal engineer must validate the preliminary assumptions made by the battery vendor. In this assumption validation, a question arises about the assumption of conduction between the battery cells. The vendor assumed perfect, thermal interface resistance free, conductance between the battery cells. This assumption is not possible but whether or not this assumption affects the results needs to be determined. The objectives of this case study are appropriate for the Bayesian-based thermal design methodology because the inputs to the system are truly uncertain. The solar flux varies as a function of time-of-year, beta angle, and thermo-optical properties. Furthermore, the internal power dissipation of the battery cells is diffi-

cult to predict at any one point in time because it depends on the state of charge of the battery, battery temperature, and spacecraft power load [45]. Certainly these variables can be bounded by a stacked worst case analysis, but this scenario is unrealistically conservative given all of the uncertainties. Moreover, a global sensitivity analysis provide resolution to the second objective of validating assumptions. GSA does not provide an answer for whether or not the assumption is correct, but given a conservative estimate of parameter ranges, it shows whether or not the parameter really affects the model output.

Table 4.2: Uncertain inputs of spacecraft battery

Parameter #	Description	Name	Units	Distribution type	Lower Bound	Upper Bound
1	Conduction coefficient of pad between batteries	G_{pb}	W/m^2-C	Uniform	2000	4000
2	Conduction coefficient of pad between batteries and side walls	G_{pw}	W/m^2-C	Uniform	2000	4000
3	Conduction coefficient of pad between batteries and top walls	G_{pt}	W/m^2-C	Uniform	2000	4000
4	Bolt conductance between walls	G_{bw}	W/C	Uniform	0.15	0.45
5	Bolt conductance between walls and radiator	G_{br}	W/C	Uniform	0.22	1.33
6	Spacecraft Temperature	T_s	C	Uniform	-20	40
7	Battery heat dissipation per cell	Q_b	W	Uniform	0	0.75
8	Solar Flux	ϕ_s	W/m^2	Uniform	1318	1422
9	Beta Angle	β	°	Uniform	-23.5	23.5
10	OSR Radiator Absorptivity	α_R	-	Uniform	0.1	0.2
11	OSR Radiator Emissivity	ϵ_R	-	Uniform	0.76	0.8

The uncertain parameters of the system are selected to ensure the objectives of the thermal design are met. These bounds will eventually be used in the uncertainty analysis, but to accurately compare the uncertainty analysis design results to the stacked worst case results, the parameter bounds must be set before any analysis is complete. The parameter bounds for the battery thermal model are shown in Table 4.2. All of the prior bounds are uniform because typical parameter ranges are not usually published with more information than just the maximum and minimum. Therefore, for conservatism, uniform bounds are chosen because no justification can be given for prior bounds of gaussian distributions with lower variances. Parameters 1-3 are the gap pad conduction coefficients. These conduction coefficients are conservatively wide estimates for the gap pad in the system as recommended by the manufacturer [46]. Parameters 4 and 5 are bolt conductances for number 6 and 8 bolts respectively. The values for these parameter bounds are taken from recommendations published in

Thompson Ramo Wooldridge Inc. (TRW) [47]. Parameter 6 is the range of typically expected spacecraft temperatures. Parameter 7 is the estimated battery heat dissipation per cell. Parameter 8 represents solar flux, which varies throughout Earth's elliptical orbit around the Sun. Parameter 9, the beta angle, comes from the orbital dynamics of a GEO satellite with a 0 degree inclination. The bounds for parameter 10, the OSR radiator's absorptivity increase for end-of-life thermo-optical properties, is derived from Figure 4.7 in Gilmore [11]. Finally, Parameter 11 captures the variability in OSR radiator's emissivity, as recommended in Gilmore [11]. All of these parameters together capture all of the dominating thermal conduction and radiation effects in the battery system.

With the thermal parameters defined, using conventional techniques, a stacked hot worst case analysis is performed to size the radiator of the battery system. For the hot worst case, all parameter bounds that increase the temperature of the batteries are chosen. Lower bounds for all of the conductances are chosen. Upper bounds are chosen for spacecraft temperature, battery heat dissipation, solar flux, beta angle, and radiator absorptivity. The lower bound is chosen for radiator emissivity. With these parameters selected, the radiator is sized to 178.5 in^2 to produce a battery temperature of 25°C, 5°C of margin to the thermal requirement. Choosing the opposite parameter bounds for the cold stacked worst case, a heater power of 63 watts is required to maintain battery temperatures to 5°C while keeping a maximum of 70% heater duty cycle.

4.2 Uncertainty Analysis

To begin the uncertainty analysis, the spacecraft battery thermal model needs to be configured to allow for the Thermal Desktop Methodology to be implemented. First, a symbol is created in the thermal model for each uncertain parameter which is passed to SINDA to be updated for each model evaluation. Of the 11 parameters, the first 7 can be implemented in the Thermal Desktop Methodology without altering the model. For parameters number 7-11, a surrogate model is required to allow for these

parameters to vary within the Thermal Desktop Methodology. Surrogate modeling can be performed in many ways but in the Thermal Desktop Methodology, a surrogate model is a Thermal Desktop model that uses alternate modeling techniques to represent model physics that are computationally intensive. Parameters number 7-11 require the model to be able to calculate variations in solar flux, beta angle, and thermo-optical properties. All of the calculations for these inputs typically require rerunning of the ray trace algorithm, which is computational intensive and not supported by the Thermal Desktop Methodology. To allow for these parameters to vary, a surrogate model is created with slight modifications. First, solar flux (ϕ_s), beta angle (β), and radiator absorptivity (α_R) are all used to calculate the heat into the system, Q_{in} , as shown in Equation 4.1.

$$Q_{in} = \phi_s \times \sin(\beta) \times \alpha_R \quad (4.1)$$

Because these three parameters are all used to calculate the heat absorbed by the radiator, a single heatload in the thermal model can accurately capture the information from all three parameters, while being allowed to vary within the Thermal Desktop Methodology. Finally, to accurately represent the varying radiator emissivity, a radiation conductor is used to capture the thermal radiation to deep space, as shown in Figure 4-2. The value of the radiation conduction can change within the Thermal Desktop Methodology, thereby approximating the changing emissivity value. Surrogate model temperature results are compared against full model results to validate the surrogate model.

With the prior uncertain parameters defined and the Thermal Desktop surrogate model created, uncertainty analysis is performed to propagate the uncertainty through the model to create the system's output PDF and CDF. 10,000 Monte Carlo model evaluations are used for the uncertainty analysis because the Monte Carlo standard error calculated from Equation 4.2 for $N = 10,000$ and p , the probability of not satisfying the temperature requirements, is $e_{mc} = 0.001$. Therefore, the Monte Carlo standard error is low enough to produce negligible impact on the results.

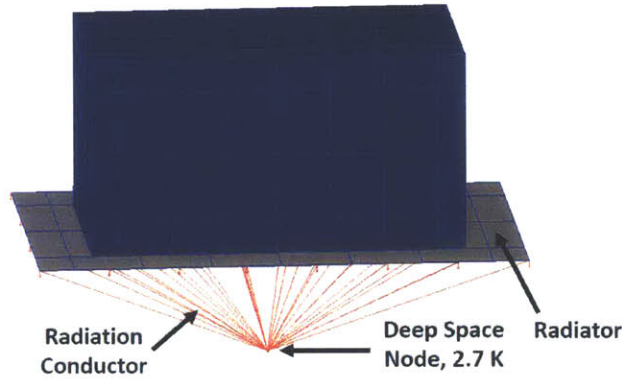


Figure 4-2: Surrogate thermal model of battery with radiation conductor

$$e_{mc} = \sqrt{\frac{p(1-p)}{N}} \quad (4.2)$$

The results of the uncertainty analysis are shown in Figure 4-3. In Figure 4-3, the blue line shows the probability of satisfying battery temperature requirements, with 5°C of margin, versus battery radiator size. The dashed black line represents the 99% confidence interval. The gray line represents the size of the radiator using conventional stacked worse case techniques. As shown, the radiator could be sized to 130 in^2 , 37% smaller than the 178.5 in^2 radiator sized using conventional techniques, and still meet the 99% confidence interval. Furthermore, sizing the radiator using these uncertainty analysis results reduces radiator size, reducing the amount of heat dissipated to space. Therefore, with the radiator sized using uncertainty analysis, the heater power required in the cold case is reduced by 17% to 54 watts. These results show how conservative the stacked worse case really is and how using uncertainty analysis to size the radiator could decrease the mass, volume, and power systems load of the battery subsystem.

4.3 Global Sensitivity Analysis Results

The next step in the Bayesian-based design methodology for the spacecraft battery is the global sensitivity analysis. The global sensitivity analysis quantitatively shows

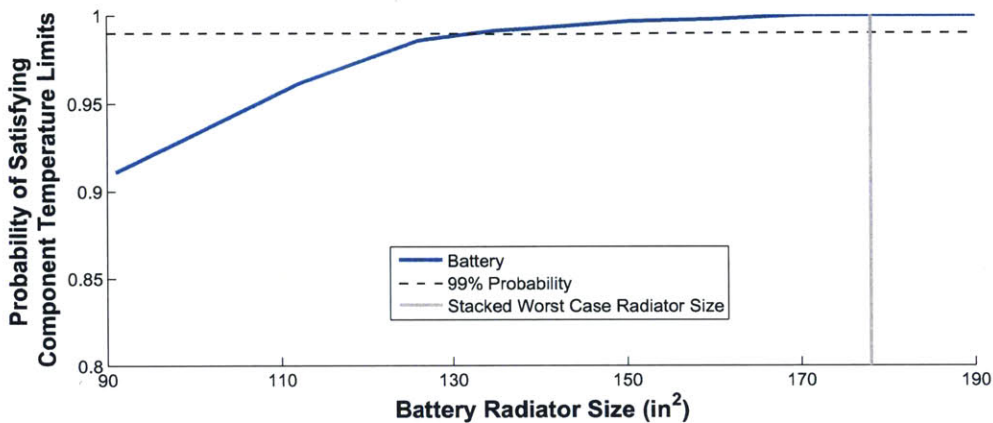


Figure 4-3: Probability of meeting spacecraft battery thermal requirement versus radiator size based on 10,000 Monte Carlo samples of the uncertain system

which parameters cause the most variance in the system’s output. Using the same thermal model and prior uncertainty bounds for the uncertain parameters, the main effects Sobol’ indices are calculated for the spacecraft battery and shown in Figure 4-4. Figure 4-4 shows the output variance’s sensitivity for each uncertain parameter input. Surprisingly, the temperature of the spacecraft, T_s , dominates the output variance. The design of the battery chassis is intended to thermally isolate the subsystem from the spacecraft as much as reasonably possible. Even with this thermal isolation, the large temperature swing of the spacecraft from -20°C to $+40^{\circ}\text{C}$ causes the most variance in the battery temperature.

In calculating which parameters most affect the variance in model output, the thermal engineer gains more information to use in the design process. With the results of the first global sensitivity analysis pass, care can be taken in the design to 1) further isolate the battery subsystem from the spacecraft, and 2) reduce the variance in spacecraft temperature near the mounting points of the battery. With these design changes in place, the results of recalculating the Sobol’ indices are shown in Figure 4-5. Figure 4-5 shows the uncertainty in battery temperature is primarily driven by the beta angle, internal dissipation of batteries, and absorptivity of the radiator. This GSA result aligns with the conclusion from Peabody et al. [15], that systems are typically driven by internal power dissipation and environmental heat

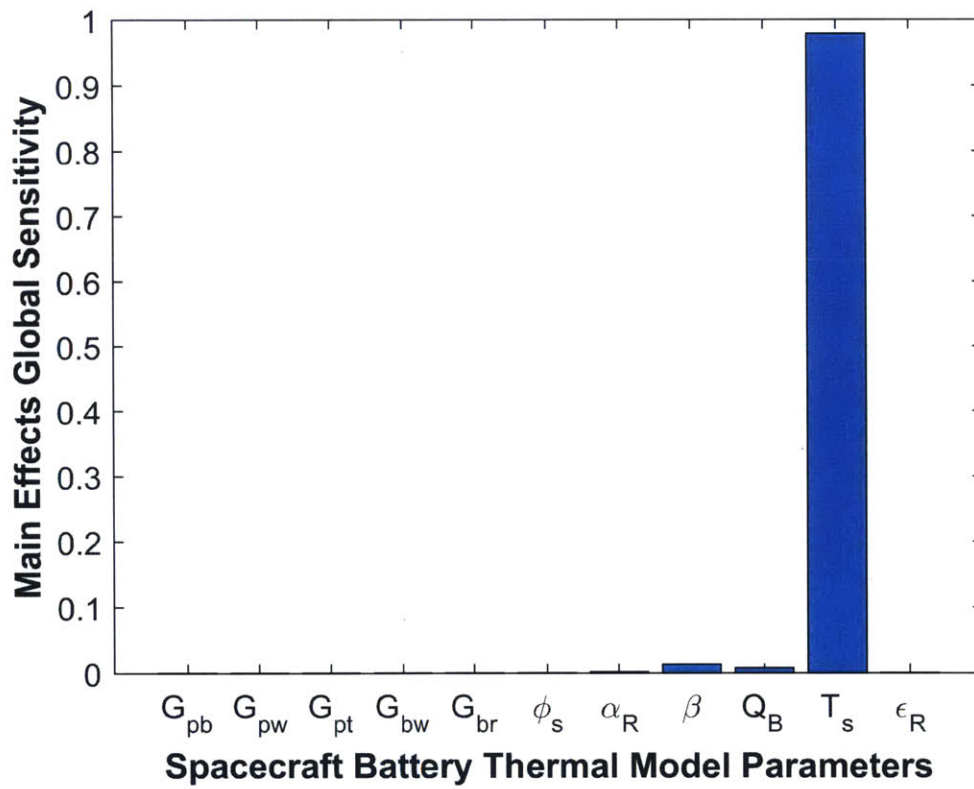


Figure 4-4: Global sensitivity analysis results of the main effect Sobol' indices of the spacecraft battery. The parameter variable names are defined in Table 4.2.

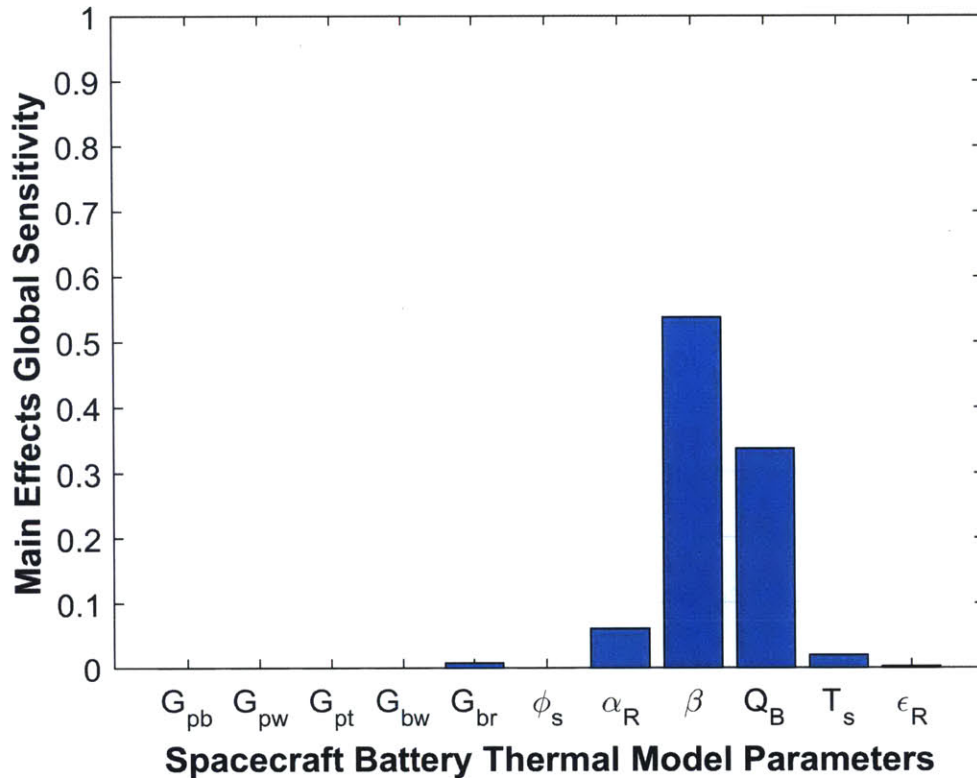


Figure 4-5: Updated global sensitivity analysis results of the main effect Sobol' indices of the spacecraft battery. The parameter variable names are defined in Table 4.2.

loads.

The information gained from performing the GSA also helps to resolve the second objective of this thermal design study. The thermal model created by the battery vendor has questionable assumptions about the conductive thermal paths between the batteries that need to be investigated. Analyzing the GSA results in Figure 4-5, the output variance created by the conduction between the battery cells through the gap pads, G_{pb} , has essentially no impact on the variance of the overall system. Therefore, the assumption of interface resistance free conductance between the batteries, although not completely correct, does not affect the output and does not invalidate the temperature results.

Chapter 5

REXIS Spectrometer Case Study

The goal of this chapter is to demonstrate the Bayesian-based design methodology implemented in Thermal Desktop on the complex 1,500 node REXIS Spectrometer thermal model as the case study. The design case study is first defined to provide context for the design problem. Thermal boundary conditions are then given for the uncertainty and global sensitivity analyses. Radiator sizing design results of the uncertainty analysis are compared against the design obtained using conventional techniques. A global sensitivity analysis using Sobol' indices is performed to gain more insight into the design of the Spectrometer. Finally, the information from the uncertainty and global sensitivity analyses is analyzed to see how this information would have affected decisions made during integration and testing if the analysis results had been obtained earlier.

5.1 Problem Definition

Before analyzing the uncertainty or global sensitivity analysis results of the REXIS Spectrometer, it is necessary to fully scope out the problem and design objectives. There are many important design parameters in the Spectrometer, but one of the critical thermal design decisions is the size of the radiator. As explained in Section 2.3, the top half of the Spectrometer, including the CCDs and radiator, is thermally isolated from the bottom half. Therefore, the temperature of the upper half of the

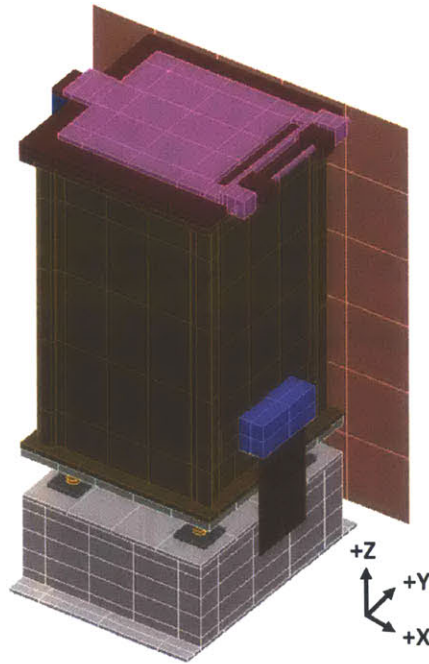


Figure 5-1: REXIS Spectrometer Thermal Desktop model

instrument is, in part, driven by the size of the radiator. The CCDs are thermally coupled directly to the radiator, which is passively cooled through thermal radiation to space. A bigger radiator cools the CCDs more and provides additional margin to the hot thermal requirement of the imagers, but increases the size and mass of the instrument. The radiator consists of a 0.0625 inch thick aluminum panel with a high emissivity white paint coating the exterior surface. Because the radiator is a large thin structure, it creates one of the lowest vibrational modes of the instrument. Any increase in radiator size negatively impacts the structural stiffness. Therefore, the radiator must be sized appropriately to meet the CCD thermal requirements, but any margin on this radiator size negatively affects the rest of the system.

The radiator on the Spectrometer is sized using conventional techniques. The Spectrometer thermal model, shown in Figure 5-1, is integrated into a model of the full spacecraft to accurately capture the spacecraft's thermal effects on REXIS. Stacked worst case hot conditions are assumed, including maximum spacecraft interface temperatures, maximum solar flux, end-of-life thermo-optical properties, maximum instrument power dissipation, and maximum e^* of MLI blankets. This stacked worst

case occurs during the cruise period when the radiation cover is closed and the radiation cover heater circuit is operating, further warming up the Spectrometer. Utilizing the full spacecraft thermal model and designing to the stacked worst case assumptions with an additional 5°C of analysis margin, the radiator area is sized to 124 in^2 . This radiator area ensures the CCDs do not get warmer than -65°C in the stacked worst hot case.

A major step in defining the problem is to select which parameters are uncertain and set each parameter's prior bounds and probability density profiles. The engineer needs to take caution in this step; all of the parameters that are uncertain and may affect the output need to be included in the analysis. Conversely, if every parameter that can possibly change at all is included, the model dimensionality would be prohibitively large. Parameters that are known to have no effect or extremely low uncertainty should not be included as uncertain parameters. For example, component mass and specific heat, C_p , do not affect the results of a steady state thermal solution. Also, the thermal conductivity of different grades of aluminum is very well known and allowing this conductivity to vary within the conductivity's small variance will not affect the model output. Therefore, component specific heats and material conductivities are included in the Spectrometer thermal model but left as fixed parameters.

The goal of the uncertain parameter selection for the Spectrometer is to include any parameter that may have an effect on any of the three thermal requirements listed in Table 2.3. The three QoIs listed in Table 2.3 are the CCDs, frangibolt, and PCBs temperatures. The goal of the design study is to size the radiator. Since the PCBs are highly conductively coupled to the temperature of the spacecraft interface and the top half of the Spectrometer is thermally isolated from the bottom half, the size of the radiator does not impact the PCB temperatures. Therefore, the PCBs QoI is not included in this Bayesian-based radiator design study. Conversely, the CCDs and frangibolt temperatures are directly correlated to the size of the radiator because the radiator cools down the upper half of the Spectrometer.

The uncertain parameter selection and bounds is performed next. The bounds of

each uncertain parameter are chosen based on the engineering model (EM) test and correlation data. The bounds are chosen utilizing the final results from the model correlation for each parameter, along with the initial expected parameter value. Table 5.1 shows the uncertain parameters defined in the Spectrometer model, along with their prior PDF bounds and profiles. Parameter 1 represents the conductive thermal joint between the radiation cover and mask frame that is created by the preload of the frangibolt. Parameter 2 is the conductance of the thermal strap that conductively couples the CCDs to the radiator. Parameters 3-7 represent all of the major bolted interfaces in the Spectrometer. Parameters 8 and 9 capture the uncertainty of the ϵ^* of the Spectrometer MLI blankets. Parameter 10 bounds the Spectrometer spacecraft interface temperatures, given to the REXIS team by the OSIRIS-REx team. Parameter 11 captures the uncertainty in the heat dissipation of the PCB boards that had not been fabricated yet as of the EM test. Parameter 12 represents the changing solar flux of the cruise period as the spacecraft varies in solar distance in its elliptical orbit to Bennu. Finally, parameter 13 captures the beginning-of-life to end-of-life change of the emissivity of the radiator. The absorptivity of the radiator does not need to be an uncertain parameter in the model because the Spectrometer is behind a sunshade and does not receive sunlight during the cruise phase while REXIS is operating and expecting to be taking science data. These 13 parameters account for the uncertainties in all of the major radiative and conductive thermal paths within the Spectrometer and between the Spectrometer and its environment.

5.2 Surrogate Model Creation

Before the uncertainty or global sensitivity analyses are completed, the Spectrometer and full spacecraft thermal models must be modified to reduce run times and allow for uncertain parameters to vary within the Thermal Desktop Methodology presented in Section 3.1.3. The full spacecraft thermal model is an extremely large and complex model that captures an adequate amount of detail when thermally designing and analyzing the OSIRIS-REx satellite, but most of this information produced from

Table 5.1: Uncertain inputs of Spectrometer

Parameter #	Description	Variable	Units	Distribution Profile	Lower Bound	Upper Bound
1	Conduction path from radiation cover to mask frame	G_r	W/in ² -C	Uniform	0.07	0.12
2	Conductance of thermal strap	G_r	W/C	Uniform	0.45	0.55
3	Conduction path from titanium TIL bolts	G_{bt}	W/C	Uniform	0.2	1.0
4	Conduction path from torlon TIL bolts	G_{bo}	W/C	Uniform	1.4	1.8
5	Conduction path mask frame to tower bolts	G_{bm}	W/C	Uniform	0.40	0.75
6	Conduction path between electronics box walls bolts	G_{be}	W/C	Uniform	1.30	1.73
7	Conduction path between DASS and tower bolts	G_{bd}	W/C	Uniform	1.30	1.73
8	e* of tower wrap MLI	e_t	-	Uniform	0.03	0.05
9	e* of radiation cover MLI	e_r	-	Uniform	0.03	0.05
10	Spacecraft interface temperature	T_s	C	Uniform	-25	50
11	Heat dissipation of MEB	Q_M	W	Uniform	6.43	8.46
12	Solar flux	ϕ_s	W/m ²	Uniform	700	2322
13	Radiator emissivity	ϵ_R	-	Uniform	0.88	0.92

the model does not pertain to REXIS. Therefore, to reduce analysis run times and to simplify the model, a surrogate model of the main spacecraft is created, shown in Figure 5-2. The surrogate model accurately represents the structures of the spacecraft deck, solar panels, and sun shade. All of the other secondary payloads and spacecraft structures that surround the Spectrometer and provide thermal radiative shading from deep space are represented using simplified rectangular surfaces of approximate shape and size.

Once the full Spectrometer thermal model is integrated into the surrogate spacecraft model, both structures need to be slightly altered to allow for the uncertain parameters listed in Table 2.3 to vary. First, a symbol is created in the model for each uncertain parameter. Thermal Desktop passes these symbols to SINDA to allow the parameters to be updated for each model evaluation. All of the parameters that are allowed to change without necessitating a dynamic SINDA run are output to SINDA. These parameters include all of the conductances, MLI e*'s, spacecraft interface temperatures, and heat dissipations.

In a typical Thermal Desktop model, solar flux cannot be changed without rerunning the ray trace algorithm, and therefore violating the constraints of the Thermal Desktop Methodology. So to accurately capture the varying solar flux, parameter 12 in Table 2.3, the full model is run to determine the temperatures of the solar arrays, sunshade, and spacecraft deck for varying solar flux levels. Then, in the surrogate

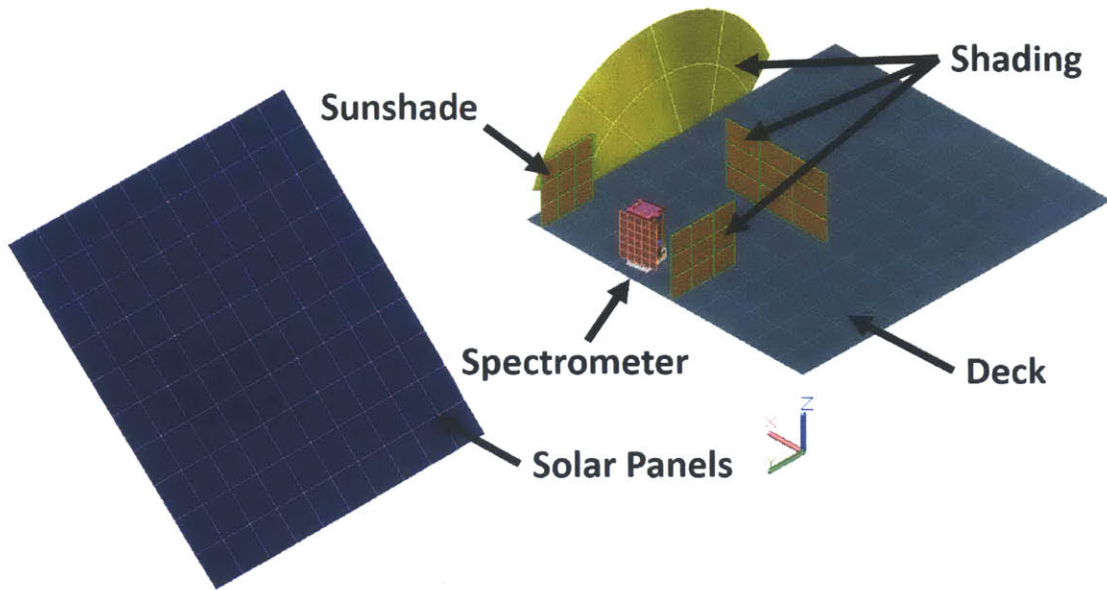


Figure 5-2: Full Spectrometer thermal model with surrogate spacecraft thermal model

model, these structures are modeled as boundary nodes with predetermined temperatures. Therefore, when the randomly generated model inputs select different solar flux levels, all the surrogate model needs to do to accurately capture this effect is to change the temperature of the boundary nodes corresponding to the solar flux level. This boundary node temperature change does not necessitate a rerunning of the ray trace algorithm and is supported by the Thermal Desktop Methodology.

Furthermore, a change in a surface's emissivity, for parameter number 13 in Table 2.3, does typically require reshooting rays. To represent this radiator emissivity variation, a radiation conductor is created in the model, shown in Figure 5-3. The radiation conductor thermally connects the radiator to a boundary node with a fixed temperature of 2.7 Kelvin, which represents the temperature of deep space. Then, changing the radiator's emissivity simply requires a change in the conductance value of the conductor.

With the simplification of the full spacecraft model to the surrogate model and the approximations of solar flux and radiator emissivity degradation, it is important to ensure the model is still producing accurate temperature results. Using the Spectrometer model that is integrated into the full spacecraft thermal model as the truth

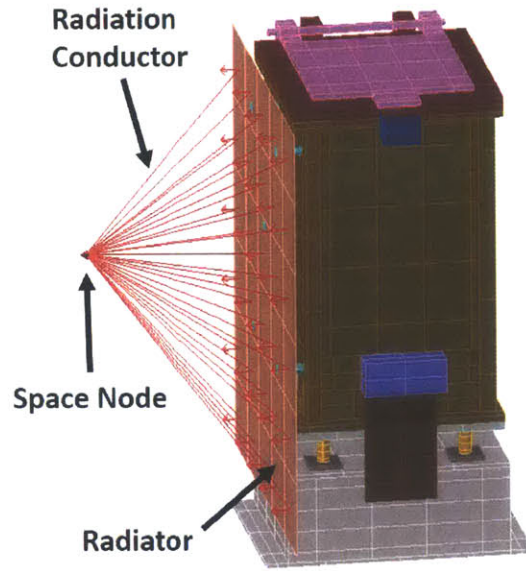


Figure 5-3: Radiation conductor to space node, used to represent uncertain emissivity of radiator

measurement, temperature output comparisons are made between the full model and the model used for the uncertainty analysis. Evaluation data points are chosen at the stacked worst hot and cold cases along with a few intermediate cases. After slight iterations on the shading surfaces shape and size and amount of rays shot for the ray trace algorithms, all of the cases correlate well to the full model, with the maximum component temperature difference being only 0.2°C and the majority of the correlation points being closer to an exact match, as shown in Table 5.2. This close correlation of data points gives high confidence in the surrogate model accuracy.

Table 5.2: Correlation results between surrogate Spectrometer and spacecraft model with full Spectrometer and spacecraft model in $^{\circ}\text{C}$

Cases	Model Temperature Comparison ($^{\circ}\text{C}$)			
	Full Model		Surrogate Model	
	CCDs	Frangibolt	CCDs	Frangibolt
Stacked worst case hot	-70.8	-10.3	-70.6	-10.2
Hot case	-75.5	-14.8	-75.4	-14.8
Cold case	-78.9	-17.7	-78.8	-17.6
Stacked worst case cold	-81.8	-19.6	-81.8	-19.5

5.3 Uncertainty Analysis

Uncertainty analysis is used to quantitatively show how well the design performs, given model uncertainties, when compared to the thermal requirements. Conventional techniques of sizing the Spectrometer radiator to the stacked worst case analysis, producing a radiator size of 124 in^2 , do not take into account how often or realistic that bounding case is. To resolve this issue, uncertainty analysis probabilistically quantifies the system output and produces a probability distribution function of model output. The engineer then applies margin in an informed and systematic way instead of indiscriminately applying the standard recommended margin that may or may not be applicable to the system in design. With this uncertainty analysis complete, the REXIS thermal engineer can design the radiator size without overdesigning the area by having more information about the system during the design process.

With the prior uncertain parameters defined and the Thermal Desktop surrogate model created and correlated, uncertainty analysis is performed to propagate the uncertainty through the model to create the system's output PDF and CDF. Similar to Chapter 4, 10,000 model evaluations are used for the uncertainty analysis to ensure a Monte Carlo error of only $e_{mc} = 0.001$. To complete this uncertainty analysis, the surrogate model is a critical tool because it brings each model evaluation time down from ~ 5 minutes to 0.0625 seconds. Even if the full model only took 1 minute per evaluation, these 10,000 model evaluations would take approximately 7 days to complete. Instead, using the surrogate model and the Thermal Desktop Methodology, the computational time for the uncertainty analysis is only 10 minutes.

The results of the uncertainty analysis are shown in Figure 5-4. Figure 5-4 shows the probability of satisfying component temperature limits versus the Spectrometer radiator size. The CCDs and frangibolt QoI are shown in blue and red respectively. The CCDs thermal requirement includes the 5°C of analysis margin that was incorporated in the original design. The dashed black line representing the probability confidence interval is set at 99% for this case study. This threshold can be set higher or lower and should be project specific based on the risk classification of the mis-

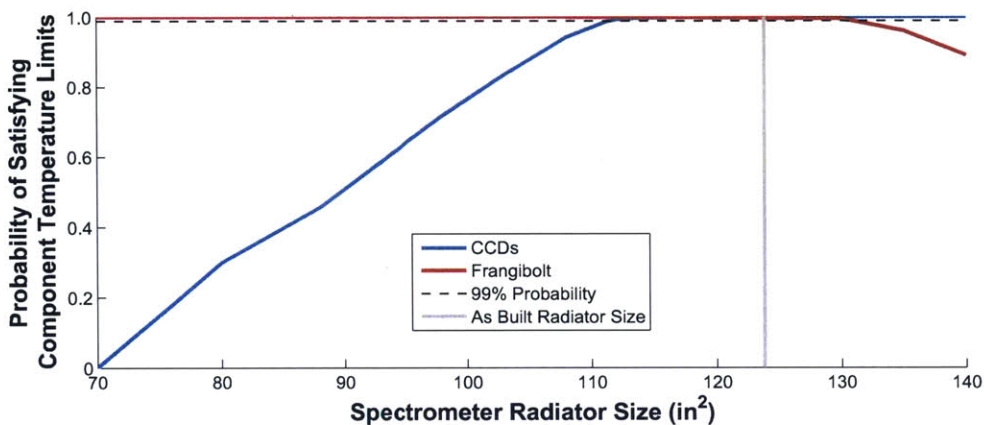


Figure 5-4: Probability of meeting Spectrometer thermal requirements versus radiator size based on 10,000 Monte Carlo samples of the uncertain system

sion. The gray line represents the 124 in^2 radiator size as it was designed and built. These data show the radiator is sized to provide 100% confidence that the thermal requirements are met in any possible thermal scenario during the Cruise phase. Not surprisingly, the conventional stacked worst case design methodology that was used to size the radiator drove an overdesign in area by 11% as the uncertainty analysis results show the CCDs probability of success crossing the 99% confidence at 111.5 in^2 radiator size. If the project's risk posture had decided to not include the 5°C of margin, the radiator size could have been reduced by 30% and still meet the 99% probability of requirement satisfaction of the CCDs. If this methodology had been implemented during the design phase, more information would have been available to the thermal engineer to allow for a less conservative radiator sizing.

Another interesting outcome from analyzing the uncertainty analysis data shows that a radiator size too large would not only produce adverse effects on the stiffness of the structure, but would also cause thermal requirement violations. The data show that the CCDs and frangibolt are at odds against one another. A radiator size too large provides significant margin to the CCDs upper temperature limit, but also cools the tower structure so much the radiation cover heater circuit can not keep the frangibolt warm enough to satisfy its lower temperature limit. The opposite effect occurs if the radiator is too small. As the radiator is designed, it falls within this

zone where both requirements are satisfied.

5.4 Global Sensitivity Analysis

The next step in the Bayesian-based design methodology for the Spectrometer is the global sensitivity analysis. The uncertainty analysis provides information on the variability of the model output due to the uncertain parameter inputs, but a global sensitivity analysis quantitatively determines which of the uncertain parameters cause the most variability in the output. With the GSA results, future testing and uncertainty reduction efforts can then be focused on the parameters that are causing the most variance in the output. Because of the high computational cost of calculating the Sobol' indices, the same surrogate model used for the uncertainty analysis is utilized in the global sensitivity analysis. The same prior uncertain parameter bounds utilized for the uncertainty analysis are used to produce the GSA results. Figure 5-5 shows the calculation of the main effects Sobol' indices for each uncertain parameter in the Spectrometer thermal model for the CCDs and frangibolt QoIs. The radiator area is kept fixed at the as-designed size and is therefore not included in the GSA results. The parameter variable names are defined in Table 5.1. The data show the uncertainty in the frangibolt is dominated by G_f . G_f is the conductance from the radiation cover to the mask frame that is created by the preload of the frangibolt. This GSA result is intuitive because, as explained in Section 2.3.4, the heater circuit, intended to warm the frangibolt and cover actuation mechanism, is epoxied to the radiation cover. The only way for the heat to transfer down to the frangibolt is 1) radiatively, 2) conduction through the cover hinge, and 3) conduction through the frangibolt preloaded joint. The surfaces on the bottom side of the radiation cover and inside of the tower all have low emissivities to help prevent parasitic heat from warming up the CCDs so radiation is not an effective heat transfer method. Moreover, the conduction through the hinge is very low because of the physical nature of the rotating joint. G_f is left as the only means to effectively transfer the radiation cover heat to the frangibolt and therefore any uncertainty in G_f dominates the variance in

frangibolt temperature.

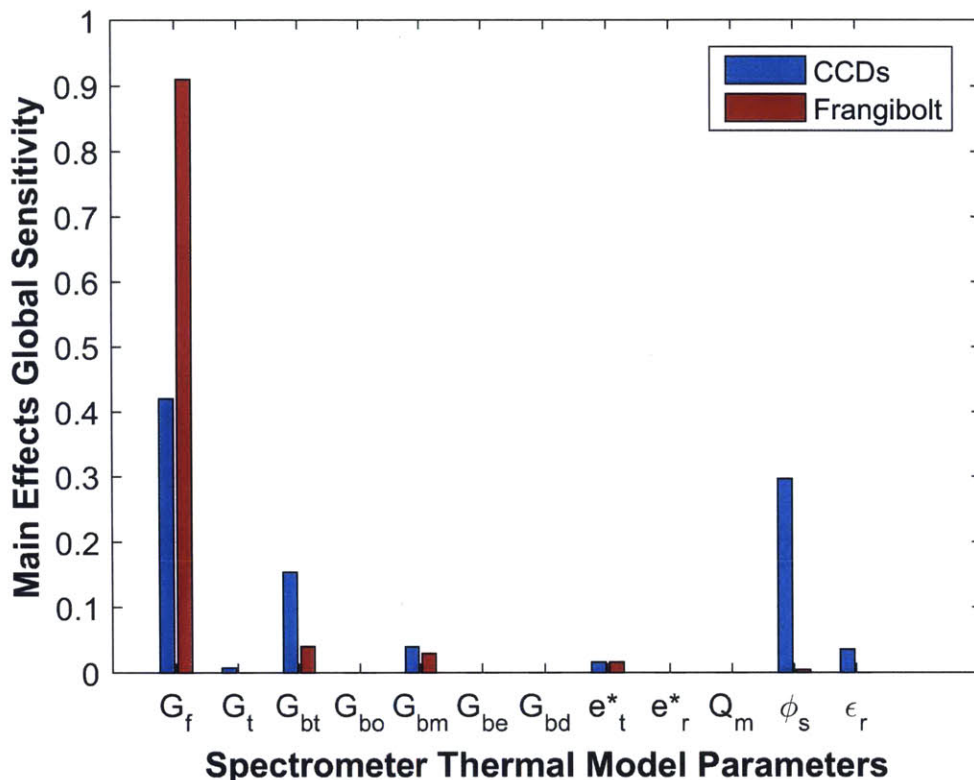


Figure 5-5: Global sensitivity analysis results of the main effect Sobol’ indices of the Spectrometer CCDs and Frangibolt QoIs. The parameter variable names are defined in Table 5.1.

For the CCDs, a more restrictive QoI, the GSA results show most of the output variance contributions are spread out over G_f , ϕ_s , and G_{bt} . It is intuitive that ϕ_s , the varying solar flux, creates variance in the temperature of the CCDs because the solar flux directly drives the temperature of the solar arrays. The solar array’s view factor to the radiator, along with the wide range of temperatures created by the wide range of solar flux, cause the temperatures of the CCDs to vary. Moreover, G_{bt} , the conductance path created by the titanium TIL bolts, creates variance in CCD temperatures because the titanium TIL is the major conductive thermal break that isolates the relatively warm electronics box from the colder upper half of the Spectrometer. The more conductive this path is, the more heat leaks into the tower, warming up the CCDs. A result of the CCDs GSA that is not necessarily intuitive

is the high sensitivity to G_f . Investigating this result shows that because the thermostats, which control the heaters, are epoxied to the radiation cover, the radiation cover is always, on average, near the midpoint of the thermostat setpoints. However, variations in G_f cause more or less heat to be dissipated into the tower structure to keep the cover at the thermostat midpoint temperature, thereby creating variance in the CCD temperature.

The Spectrometer CCDs GSA results would have been useful during integration and testing. During the first vibration test of the flight model Spectrometer, modal shifting occurred. This modal shifting was determined to be caused by under-torqued bolts in the titanium TIL. During the investigation, it was realized that the fasteners had not been thoroughly analyzed. Analysis showed that higher torques than were used on the EM were appropriate to provide margin to the vibrational loads. Due to schedule pressure, ramifications caused by increasing the fastener torques were not considered. During the flight TVAC test, these higher TIL torques increased the thermal conductance from the warm electronics box to the cold tower, warming up the CCDs by 5-10°C. If the CCDs GSA had been performed prior to the flight vibration test, knowing the CCDs sensitivity to the TIL bolted interfaces could have made the team more attentive to the potential thermal ramifications of increasing the fastener torque values. For more information on the vibration test anomalies see Bayley [34].

5.5 Frangibolt Thermal Vacuum Testing Anomaly

The events of the REXIS flight thermal vacuum test corroborate the global sensitivity analysis results, namely that G_f , the conductance from the radiation cover to the mask frame, which is created by the frangibolt preload, dominates the uncertainty in the frangibolt temperature. The TVAC test performed at the Applied Physics Laboratory was performed on the flight REXIS Spectrometer and SXM. The test configuration, shown in Figure 5-6, is intended to replicate the flight scenario as accurately as possible. Two thermally controllable plates, one each for the Spectrometer and

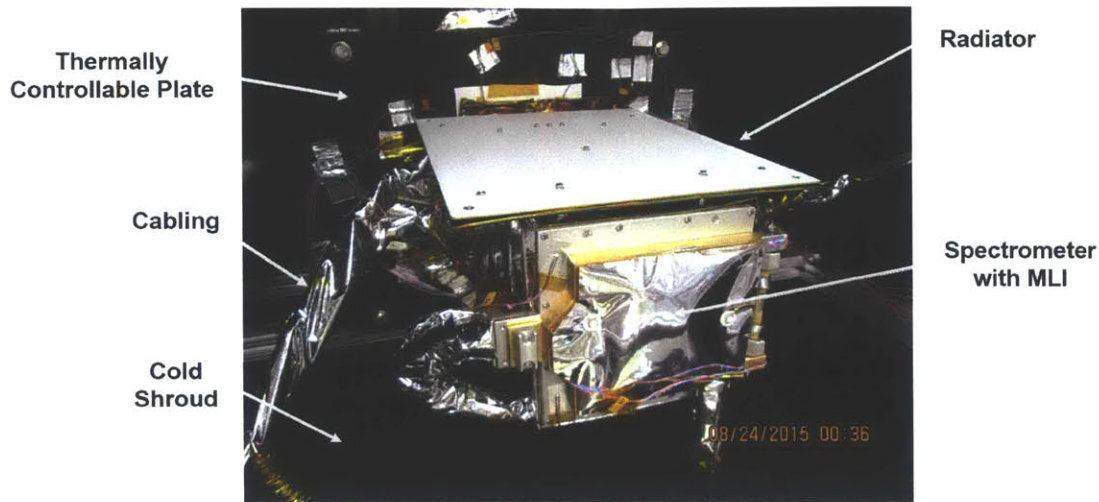


Figure 5-6: Spectrometer mounted in the thermal vacuum chamber

SXM, are mounted inside the chamber to represent the spacecraft interface temperatures. The black painted wall surrounding the chamber is cooled to liquid nitrogen temperatures to simulate radiative coupling to deep space. Although the second and third order effects of the radiative coupling to the other instruments mounted near the Spectrometer are not captured, the important first order effects of the conduction to the spacecraft interface and thermal radiation to space are captured accurately. As per the GEVS recommendations, the TVAC test cycled the instruments 8 times using the temperature controllable baseplates.

Early on in the test the temperature of the frangibolt housing was noticed to be dipping below the -20°C limit. This anomaly was not an immediate threat to the safety of the hardware because the frangibolt was still well within the published operational and survival limits, as shown in Figure 5-7. Figure 5-7 shows the temperatures of the radiation cover, frangibolt housing, and tower for the entire duration of the TVAC test. Unexpectedly, different than the EM TVAC test, the temperature of the frangibolt housing was closer to the temperature of the tower and not well correlated to the temperature of the radiation cover. Even with the colder than expected temperatures of the frangibolt housing, the frangibolt housing was still above the published operational and survival temperature ranges. Nevertheless, the overcooling of the frangibolt is an issue for on orbit operations because of the desire for long term

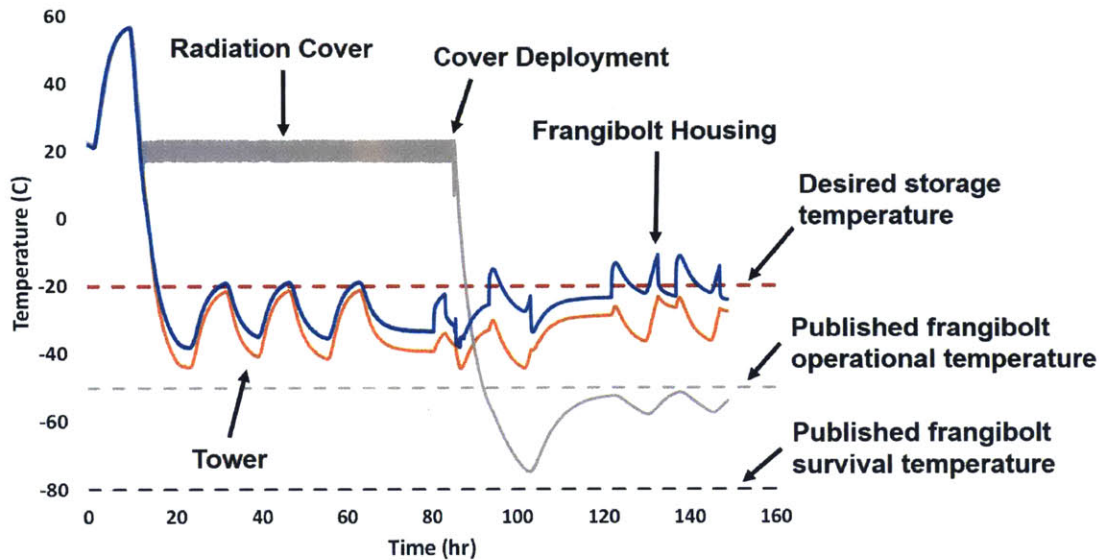


Figure 5-7: Temperature of the frangibolt housing, radiation cover, and tower for the duration of the REXIS flight TVAC test

storage at -20°C and a root cause investigation was started.

Because the frangibolt housing is intended to be warmed via the heater circuit on the radiation cover, the root cause investigation started by discussing possible deviations in the flight hardware compared to the EM hardware. One of the team members recalled the possibility of poor flatness in the tongue of the flight radiation cover during assembly. Pictures of the hardware, shown in Figure 5-8, were taken only after the frangibolt was installed, which shows the cover flush against the mask frame. To test this poor radiation cover flatness hypothesis, the predicted radiation cover heater duty cycle was compared to the actual duty cycle seen during the TVAC test. The analysis predictions were created using the thermal model that was correlated to the EM test results that did not have this overcooling issue. The results of this comparison are shown in Figure 5-9.

The results from Figure 5-9 corroborate the radiation cover poor flatness hypothesis. The comparison between the transient behavior of the two duty cycles provides the critical information. If the radiation cover was slightly bent up during installation, part of the frangibolt preload would be applied to deforming the cover down flat and therefore the thermal conductance, G_f , would be lower. Analyzing the data

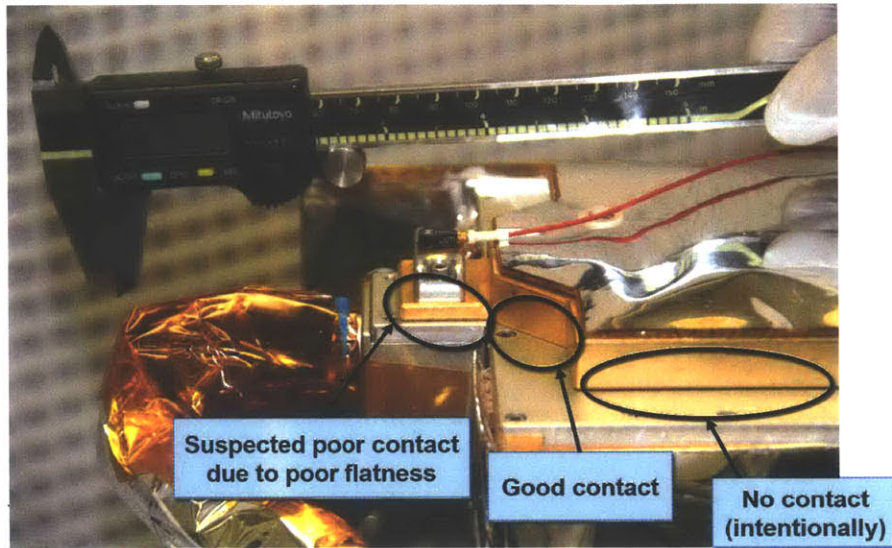


Figure 5-8: Radiation cover with frangibolt installed prior to TVAC testing

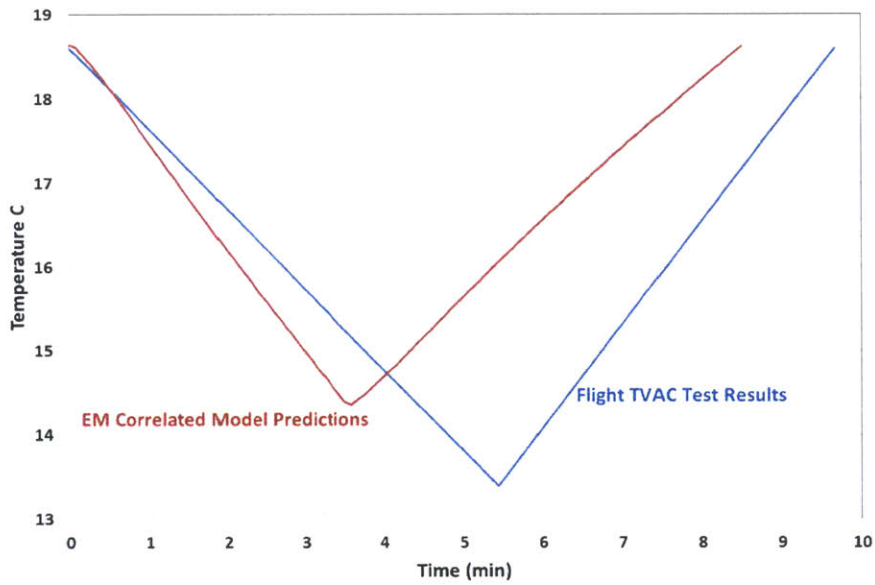


Figure 5-9: Comparison between model predicted radiation cover heater duty cycle with actual test results

in Figure 5-9, the flight configuration takes longer to cool down because the warm radiation cover is less coupled to the cold tower. Moreover, the slope of the flight configuration heating up is steeper because the radiation cover is more isolated and therefore has effectively less mass to heat up. Both of these results indicate a lower conductance through the frangibolt joint. The thermal model was correlated to the ongoing flight TVAC test by reducing the G_f conductance. The correlation results are shown in Figure 5-10 and Table 5.3. Figure 5-10 shows the cool down and heat up rates of the duty cycles to be a much better match. Table 5.3 shows how far off the original predictions were and how the updated model correlates well to the test results.

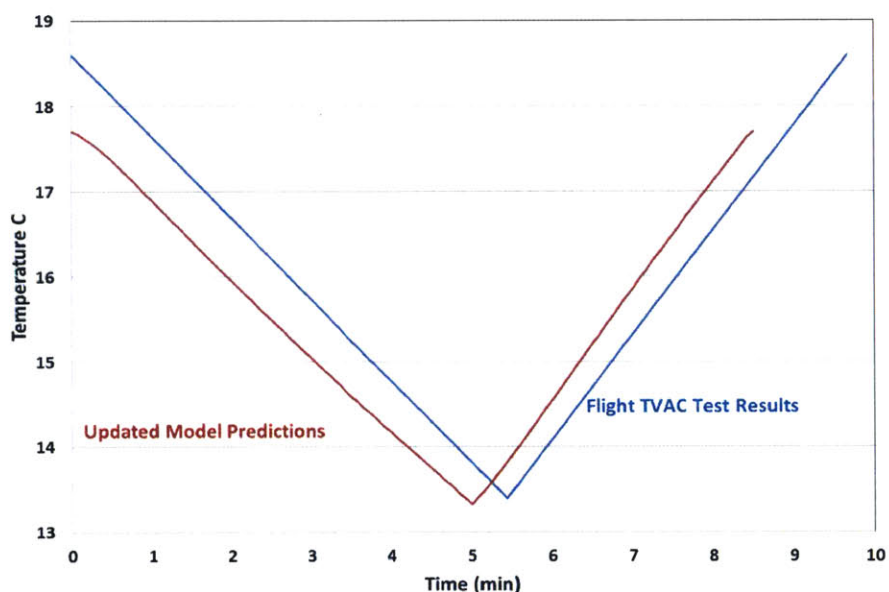


Figure 5-10: Comparison between updated model predicted radiation cover heater duty cycle with lower G_f and actual test results

Once the root cause is identified, a solution to this frangibolt overcooling issue must be implemented for flight that is minimally invasive but also effective. Because the lower conductance through the radiation cover to mask frame joint is the root cause of the issue, any change to the radiation cover heater circuit would not be effective. Replacing the radiation cover with the spare cover is the most invasive solution, and therefore not a viable path forward. An effective and minimally invasive

Table 5.3: Comparison of averaged steady state temperatures between the EM correlated thermal model, updated thermal model, and flight TVAC test results

Case	Cover (°C)	Frang Housing (°C)	Mask Frame (°C)	Truss -X (°C)
TVAC Test	16	-38	-40	-44
EM Correlated	17	-12	-15	-34
Updated FM Predicts	16	-35	-37	-43

solution that is decided upon is to use the ground support equipment (GSE) heaters that are epoxied to the side of the frangibolt housing as a second heater circuit. The heaters are flight grade but were only intended to be used during testing to prevent the frangibolt from getting too cold once the cover actuation had occurred and the radiation cover heater circuit was powered off. To implement this heater circuit, an additional thermostat, with setpoints near the -20°C requirement, is added to the underside of the frangibolt housing and the circuit is spliced in parallel with the radiation cover heater circuit.

Once the TVAC test was completed and the flight hardware was removed from the thermal chamber, the anomaly investigation results were confirmed. Figure 5-11 shows a picture of the Spectrometer after frangibolt actuation. The cover is closed by hand, without the preload of the frangibolt. As shown, there is a measured 0.010 inch to 0.020 inch gap between the tongue of the radiation cover and the mask frame which caused the G_f conductance joint to be lower than expected from the EM hardware.

The uncertainty and global sensitivity analysis results presented in this chapter provide the REXIS thermal engineer with more information about the Spectrometer. The GSA results clearly show the dominating uncertain parameter in the system for the frangibolt temperature is G_f , the thermal joint created by the frangibolt preload. If this information had been conveyed to the REXIS team earlier, the overcooling issue potentially could have been avoided through a more rigorous inspection of the hardware or tighter machining tolerances. This REXIS Spectrometer case study is an example of how the Bayesian-based design methodology can be used to help

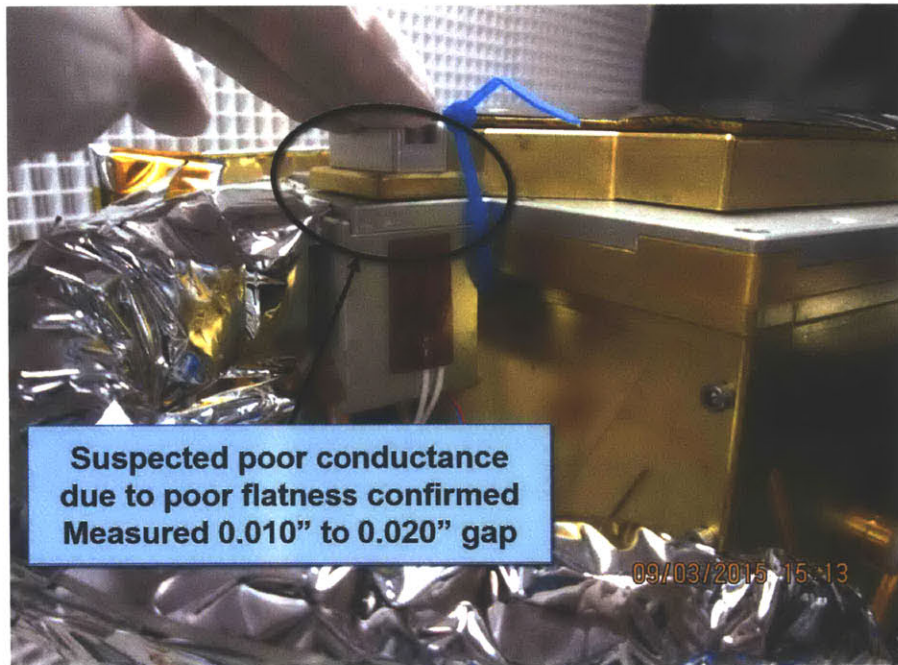


Figure 5-11: Radiation cover post TVAC test after cover actuation has taken place and frangibolt preload no longer present. Cover is closed only by hand

engineering teams make more informed decisions and aid in the prevention of thermal overdesign.

Chapter 6

Conclusion

6.1 Thesis Summary

As satellite design has increased in complexity, thermal engineers in industry have continued to utilize the same conservative design techniques that have been employed for years. The traditional conservative approach of designing to the stacked worst case with additional margin does typically produce a successful thermal control system, but comes at the price of added cost, lead time, mass, size, and power. This conservative approach arises out of the lack of system knowledge about the uncertainty associated with thermal input parameters. To reduce the conservatism in thermal design, Bayesian-based methods can be used to more rigorously quantify and account for the parametric uncertainty. Part of the reason why Bayesian-based methods are not the industry standard is because of the typically high computational cost associated with these techniques and thermal modeling run times. Therefore, to bridge the gap between these state-of-the-art techniques and the industry standard, this thesis develops a methodology to reduce simulation time and implement these analysis techniques in the industry standard software, Thermal Desktop.

Three case studies are presented in this thesis to demonstrate that the Bayesian-based design methodology can be implemented in Thermal Desktop with tolerable computational time. The first case study, presented in Chapter 3, is performed on the relatively simple 65 node REXIS Solar X-ray Monitor thermal model. Bayesian-

based design techniques have already been applied to the SXM in recent publications, but the published work performed the analysis on a simplified model in Matlab. To verify the proper implementation of the Thermal Desktop Methodology, the analysis was re-performed in Thermal Desktop with a more discretized model but identical boundary conditions. The results between the two models correlate well and the slight discrepancies are accounted for in the models' differences. The close correlation of the results provide confidence in the Thermal Desktop Methodology. The second case study, presented in Chapter 4, is performed on a moderately complex 650 node representative spacecraft battery thermal model. The case study details all of the steps of the Bayesian-based design methodology, including problem definition, uncertain parameter selection, surrogate model creation, uncertainty analysis, global sensitivity analysis, and evaluation of analysis results. Compared to the conventional stacked worst case radiator sizing, the uncertainty analysis results show the radiator could be sized 37% smaller and still meet the 99% confidence interval for all thermal cases. Furthermore, the global sensitivity analysis results show the battery temperatures have a high sensitivity to spacecraft interface temperatures. If the spacecraft interface temperature can be reduced in variance, a second pass of GSA shows the parameters causing the most amount of output variance are beta angle, internal battery dissipation, and radiator absorptivity. Finally, the third case study, presented in Chapter 5, is performed on the complex 1,500 node REXIS Spectrometer thermal model. Comparing the uncertainty analysis results to the radiator sized using conventional techniques, the radiator could have been sized 11% smaller and still have a 99% probability of meeting the thermal requirements during all mission phases. Furthermore, the GSA results showing the criticality of one uncertain parameter in the model could have been used to avoid issues experienced during integration and testing. These case studies of increasing model size and complexity demonstrate the applicability of the Bayesian-based design methodology to larger spacecraft systems in the industry standard software.

6.2 Applicability of Bayesian-based Design Methodology

Bayesian-based design is not expected to revolutionize thermal engineering of spacecraft but rather to provide the thermal engineer with more tools to aid in the reduction of overdesign. This design methodology is most appropriate for payloads that are highly constrained in mass, volume, and/or power because it provides a quantitative technique to reduce the design conservatism while still allowing for a high probability of success. Even on spacecraft where mass, volume, and/or power are not the driving factors, these design tools still provide the thermal engineer with more knowledge about the system. This additional system knowledge helps the engineering team make more informed decisions on the design and testing of hardware, reducing the probability of encountering potential issues in all phases of the satellite design and implementation.

Even with the Thermal Desktop Methodology's model run time reduction advancements, limitations do exist which do not make this methodology applicable to the thermal design of every satellite. The methodology presented here only supports thermal analyses that can be represented through a steady state analysis. Furthermore, overly complex models that require significant simulation time and cannot be reduced through the use of surrogate models are not applicable for this design methodology. Moreover, the design methodology presented here is not recommended for engineers who are completely new to thermal engineering of spacecraft. This recommendation is driven by the importance of the selection of uncertain parameters and their bounds. Without performing an extensive study of each possible modeling parameter, the thermal engineer needs to rely upon experience and intuition to identify which parameters in the model should be uncertain. If a parameter with high variance is left as a fixed parameter in the Bayesian methodology, the results produced will be inaccurate.

6.3 Contributions and Future Work

The major contribution of this thesis is the development of a methodology for previously established Bayesian-based analysis techniques to be implemented in the industry standard software for the thermal design of satellites. Being able to apply these rarely used analysis techniques in the industry standard software helps to increase the accessibility of the tools to the thermal engineers in industry. This further accessibility will hopefully lead to more widespread implementation of the Bayesian-based design tools to help in the reduction of thermal overdesign. The work done in this thesis can be extended further by:

- Further developing the Thermal Desktop Methodology to allow for the uncertainty and global sensitivity analyses to be implemented on transient thermal analyses without prohibitively long model run times
- Further developing Thermal Desktop surrogate modeling techniques to expand the capabilities of the analysis tools. Surrogate modeling techniques to expand upon include: varying solar flux over many surfaces, surface to surface radiation interactions for varying surface emissivities, and varying mass for transient calculations.
- Creating a repository for prior uncertain parameter bounds for typical thermal model inputs

Bibliography

- [1] NASA. Landsat's thermal infrared sensor (tirs) instrument. Technical report. Online accessed 2016-5-5.
- [2] Ball Aerospace. Qualification and integration of the laser transmitter for the calipso aerosol lidar mission. Technical report.
- [3] Matthew B Garrison. Statistical analysis of thermal analysis margin. Thermal and Fluids Analysis Workshop, 2011.
- [4] OSIRIS-REx. <http://blogs.solidworks.com/teacher/2014/05/solidworks-helps-to-send-your-name-to-the-asteroid-bennu.html>. [Online; accessed 2016-5-5].
- [5] Kevin Dale Stout. *Bayesian-based simulation model validation for spacecraft thermal systems*. PhD thesis, Massachusetts Institute of Technology, 2015.
- [6] NASA. Origins-spectral interpretation-resource identification-security-regolith-explorer (osiris-rex) project environmental requirements document revision h. Technical report.
- [7] TiNi FD04 Frangibolt. <http://www.tiniaerospace.com/fcfd04.html>. [Online; accessed 2016-5-5].
- [8] Can we afford our own future. Technical report, Deloitte, 2009.
- [9] Gabe Karpati, Tupper Hyde, Hume Peabody, and Matthew Garrison. Resource management and contingencies in aerospace concurrent engineering. In *AIAA SPACE 2012 Conference & Exposition*, page 5273, 2012.

- [10] Earth orbit environmental heating. Technical report, NASA Goddard Space Flight Center. GD-AP-2301.
- [11] David G. Gilmore. *Spacecraft Thermal Control Handbook*, volume 1. The Aerospace Press, El Segundo, California, 2 edition, 2002.
- [12] Wiley J Larson and James Richard Wertz. Space mission analysis and design. Technical report, Microcosm, Inc., Torrance, CA (US), 1992.
- [13] John W Welch. Rationale for mil-std-1540e thermal test requirements. Spacecraft Thermal Control Workshop, 2011.
- [14] General environmental verification standard. Technical report, NASA Goddard Space Flight Center, 2005.
- [15] Hume Peabody, Juan Rodriguez-Ruiz, and Veronica Benitez. Thermal margin study for the global precipitation measurement spacecraft. In *42nd International Conference on Environmental Systems, San Diego, CA*, 2012.
- [16] Veronica Otero, Carol Mosier, and David Neuberger. Thermal infrared sensor (tirs) instrument thermal subsystem design and lessons learned. In *43rd International Conference on Environmental Systems*, page 3445, 2013.
- [17] M Donabedian. Thermal uncertainty margins for cryogenic sensor systems. In *Proceedings of the AIAA 26th Thermophysics Conference, AIAA-91-1426*, 1991.
- [18] Joseph F Gasbarre, Wes Ousley, Marc Valentini, Jason Thomas, and Joel Dejoie. The calipso thermal control subsystem. In *Proceedings of the 6th IAA Symposium on Small Satellites for Earth Observation*, 2007.
- [19] Daniel P Thunnissen and Glenn T Tsuyuki. *Margin determination in the design and development of a thermal control system*. Society of Automotive Engineers, 2004.

- [20] Andrea Saltelli, Marco Ratto, Terry Andres, Francesca Campolongo, Jessica Cariboni, Debora Gatelli, Michaela Saisana, and Stefano Tarantola. *Global sensitivity analysis: the primer*. John Wiley & Sons, 2008.
- [21] Andrea Saltelli, Stefano Tarantola, and KP-S Chan. A quantitative model-independent method for global sensitivity analysis of model output. *Technometrics*, 41(1):39–56, 1999.
- [22] Andrea Saltelli, Stefano Tarantola, Francesca Campolongo, and Marco Ratto. *Sensitivity analysis in practice: a guide to assessing scientific models*. John Wiley & Sons, 2004.
- [23] Bertrand Iooss and Paul Lemaître. A review on global sensitivity analysis methods. In *Uncertainty Management in Simulation-Optimization of Complex Systems*, pages 101–122. Springer, 2015.
- [24] Edward Beshore, Brian Sutter, Ronald Mink, Dante Lauretta, Michael Moreau, William Boynton, Jason Dworkin, David Everett, Christopher Shinohara, and Jonathan Gal-Edd. The osiris-rex asteroid sample return mission. In *Aerospace Conference, 2015 IEEE*, pages 1–14. IEEE, 2015.
- [25] Dante S Lauretta and OSIRIS-Rex Team. An overview of the osiris-rex asteroid sample return mission. In *Lunar and Planetary Science Conference*, volume 43, page 2491, 2012.
- [26] TG Müller, L O’Rourke, AM Barucci, A Pál, C Kiss, P Zeidler, B Altieri, BM González-García, and M Küppers. Physical properties of osiris-rex target asteroid (101955) 1999 rq36-derived from herschel, vlt/visir, and spitzer observations. *Astronomy & Astrophysics*, 548:A36, 2012.
- [27] PH Smith, B Rizk, E Kinney-Spano, C Fellows, C d’Aubigny, and C Merrill. The osiris-rex camera suite (ocams). In *Lunar and Planetary Science Conference*, volume 44, page 1690, 2013.

- [28] CS Dickinson, M Daly, O Barnouin, B Bierhaus, D Gaudreau, J Tripp, M Ilnicki, and A Hildebrand. An overview of the osiris rex laser altimeter (ola). In *Lunar and Planetary Science Conference*, volume 43, page 1447, 2012.
- [29] AA Simon-Miller and DC Reuter. Osiris-rex ovirs: A scalable visible to near-ir spectrometer for planetary study. In *Lunar and Planetary Science Conference*, volume 44, page 1100, 2013.
- [30] Victoria Hamilton and Philip Christensen. The osiris-rex thermal emission spectrometer (otes). In *EGU General Assembly Conference Abstracts*, volume 16, page 4687, 2014.
- [31] Branden Allen, Jonathan Grindlay, Jaesub Hong, Richard P Binzel, Rebecca Masterson, Niraj K Inamdar, Mark Chodas, Matthew W Smith, Marshall W Bautz, Steven E Kissel, et al. The regolith x-ray imaging spectrometer (rexis) for osiris-rex: identifying regional elemental enrichment on asteroids. In *SPIE Optical Engineering+ Applications*, pages 88400M–88400M. International Society for Optics and Photonics, 2013.
- [32] Office of Safety and Mission Assurance. Risk classification of nasa payloads. *NASA Procedural Requirements NPR 8705.4*, June 2014.
- [33] David Brad Carte. The regolith x-ray imaging spectrometer flight model: Structural design, analysis, and testing. Master’s thesis, Massachusetts Institute of Technology, 2015.
- [34] Laura C Bayley. Integration and test of the regolith x-ray imaging spectrometer and recommendations for low-cost, high-risk spaceflight programs. Master’s thesis, Massachusetts Institute of Technology, 2016. In progress thesis.
- [35] Pronoy Biswas. Radiation management, avionics development, and integrated testing of a class d space-based asteroid x-ray spectrometer. Master’s thesis, Massachusetts Institute of Technology, 2016. In progress thesis.

- [36] Jonathan Gal-Edd and Allan Cheuvront. The osiris-rex asteroid sample return mission operations design. In *Aerospace Conference, 2015 IEEE*, pages 1–9. IEEE, 2015.
- [37] Kusum Sahu, Henning Leidecker, and Darryl Lakins. Eee-inst-002: Instructions for eee parts selection, screening, qualification, and derating. Technical report, NASA/TP-2003-212242, 2003.
- [38] JD Busch. The frangibolt flies: using shape memory alloy on the spacecraft clementine. In *SMST-94: The First International Conference on Shape Memory and Superelastic Technologies*, pages 259–264, 1994.
- [39] Chad Fish, Charles Swenson, Tim Neilsen, Bryan Bingham, Jake Gunther, Erik Stromberg, Steven Burr, Robert Burt, Mitch Whitely, Geoff Crowley, et al. Dice mission design, development, and implementation: Success and challenges. In *26th Annual AIAA/USU Conference on Small Satellites*, 2012. SSC-12-XI-1.
- [40] David B Carte, Niraj K Inamdar, Michael P Jones, and Rebecca A Masterson. Design and test of a deployable radiation cover for the regolith x-ray imaging spectrometer. 2014.
- [41] Michael P Jones. The engineering design of the rexis solar x-ray monitor and risk management considerations for resource constrained payload development. Master’s thesis, Massachusetts Institute of Technology, 2015.
- [42] Andrea Saltelli. Making best use of model evaluations to compute sensitivity indices. *Computer Physics Communications*, 145(2):280–297, 2002.
- [43] Michela Nardo, Michaela Saisana, Andrea Saltelli, Stefano Tarantola, Anders Hoffman, and Enrico Giovannini. Handbook on constructing composite indicators. 2005.
- [44] Sanjay R Arwade, Mohammadreza Moradi, and Arghavan Louhghalam. Variance decomposition and global sensitivity for structural systems. *Engineering Structures*, 32(1):1–10, 2010.

- [45] Barbara McKissock, Patricia Loyselle, and Elisa Vogel. Guidelines on lithium-ion battery use in space applications. Technical report, NASA/TM-2009-215751, 2009.
- [46] Bergquist Gap Pad Conductivities. <http://www.bergquistcompany.com>. [Online; accessed 2016-5-5].
- [47] Anon. *Project MILSTAR Engineering Design Standards, Section 2.2*. TRW, Inc., 1984.